JOINT EUROPEAN TORUS

JET–P(90)46

O.N. Jarvis, E. Clipsham, M. Hone, B. Laundy, M. Pillon, M. Rapisarda,
G. Sadler, P. van Belle, K.A. Verschuur and JET Team

Use of Activation Techniques at JET for the Measurement of Neutron Yields from Deuterium Plasmas

Use of Activation Techniques at JET for the Measurement of Neutron Yields from Deuterium Plasmas

O.N. Jarvis, E. Clipsham, M. Hone, B. Laundy, M. Pillon[1], M. Rapisarda[1], G. Sadler, P. van Belle, K.A. Verschuur[2] and JET Team*

JET-Joint Undertaking, Culham Science Centre, OX14 3DB, Abingdon, UK

[1]Associazione EURATOM-ENEA, CRE Frascati, Italy.
[2]ECN Petten, The Netherlands.
** See Appendix 1*

Preprint of Paper to be submitted for publication in
Fusion Technology

ABSTRACT.

The time-dependence of the 2.5MeV neutron emission from JET is reliably measured using fission chambers. The absolute calibration of these chambers is required to an accuracy of 10%, or better, for a range of intensities that may cover 6 or more decades. At JET, this calibration is now achieved by use of activation techniques, the most convenient of which involves fissionable materials (thorium and uranium) and delayed neutron counting. Because delayed neutron counting is unfamiliar in the fusion community, particular care was taken to obtain confirmation of the results based on this method by comparison with measurements made using the conventional activation procedure (involving indium, nickel and zinc as target materials). As the activation measurements can be influenced appreciably by the weak emission of 14MeV neutrons, this contribution was measured separately using high threshold energy activation reactions (in copper and silicon). Neutron transport calculations are employed to relate the measured local fluences of both 2.5MeV and 14MeV neutrons to the total yields from the plasma. Absolute calibration accuracies of 6% and 8% are claimed for 2.1MeV and 14MeV neutron yields, respectively; the accuracy of the 14MeV to 2.5MeV yield ratios is 6%.

CONTENTS

		Page
1.	INTRODUCTION	1
2.	THE ACTIVATION ANALYSIS FACILITY	3
	2.1 Choice of irradiation positions	3
	2.2 The pneumatic transport system	4
	2.3 The delayed neutron system	5
	2.4 The gamma-radiation detection system	7
	2.5 Activation sample selection	7
3.	NEUTRON TRANSPORT CALCULATIONS	8
	3.1 FURNACE	9
	3.2 MCNP	9
	3.3 Comparison of code predictions	9
	3.3.1 Wall-averaged neutron fluences and nickel activation	9
	3.3.2 Activation of sections of wall taken from small circular ports	10
	3.3.3 Calculations for the use of the irradiation ends	11
4.	EXPERIMENTAL RESULTS	13
	4.1 Treatment of the fission-chamber data	13
	4.2 Treatment of the delayed-neutron data	14
	4.3 Treatment of the gamma-emission data	15
	4.3.1 2.5 MeV neutron activation	16
	4.3.2 14 MeV neutron activation	17
5.	ASSESSMENT OF UNCERTAINTIES	19
	5.1 Fission chamber yields	19
	5.2 Delayed neutrons	20
	5.3 Gamma-decay measurements	21
	5.4 Transport calculations	21
	5.5 Accuracy of final results	22
6.	DISCUSSION	22
7.	CONCLUSIONS	24
	REFERENCES	25

TABLES

		Page
I.	FURNACE and MCNP 2.5 MeV neutron fluences averaged over the surface of the first wall.	27
II.	Neutron fluences at locations from which small pieces of vacuum vessel were subsequently removed for laboratory analysis.	28
III.	Activation coefficients computed with FURNACE and MCNP for the outside (inboard and outboard) irradiation ends (2.5 MeV and 14 MeV neutrons).	29
IV.	Activation coefficients computed with MCNP for the new (inside) irradiation ends: 2.5 MeV and 14 MeV neutrons.	30
V.	Fast fission integral cross-sections and Watt-averaged DOSCROS84 values.	31
VI.	Activation characteristics and HPGe detector efficiencies for the $^{58}Ni(n,p)^{58}Co$, $^{115}In(n,n')^{115m}In$ and $^{64}Zn(n,p)^{64}Cu$ reactions for 2.5 MeV neutrons and the $^{63}Cu(n,2n)^{62}Cu$ and $^{28}Si(n,p)^{28}Al$ reactions for 14 MeV neutrons.	32
VII.	Corrections to the activation coefficients computed with MCNP, for a 20 keV Maxwellian plasma, as appropriate to the conditions for JET discharges.	33
VIII.	Results of the 2.5 MeV activation measurements, including corrections for 14 MeV neutron contribution and vessel expansion.	34
IX.	Relative responses measured in the eight irradiation ends, for 2.5 MeV and 14 MeV neutrons.	35
X.	Accuracy of neutron yield measurements.	36

FIGURES

		Page
1.	Section of JET at the horizontal mid-plane, showing the positions of the fission chambers and of the irradiation ends.	37
2.	A drawing of a vertical section through the JET vacuum vessel, showing the location of the irradiation ends.	38
3.	Illustrating the time sequence involved in the use of the delayed neutron counting system for a typical JET discharge.	39
4.	Showing the variation of the response coefficient for ^{238}U as a function of height above the tokamak horizontal midplane. The results of FURNACE and MCNP transport codes are compared and measurements of the gradient above the operating position are fitted to the MCNP data. The coefficient at 194.5 cm. is taken to be 4.74×10^{-31} ± 5%.	40
5.	Showing the cross-sections for the reactions used in the measurement of 2.5 MeV neutron fluxes; also shown are the Watt fast fission neutron energy spectrum and the Gaussian representing the 2.5 MeV neutrons from d-d fusion reactions.	41
6.	The ratio of delayed neutron/fission chamber neutron yields as a function of neutron emission strength. The solid curves indicate the ± 2 s.d. uncertainties attributable to counting statistics.	42

1. INTRODUCTION

The time-resolved neutron yield from the Joint European Torus (JET) is reliably recorded using a set of fission chambers [1] mounted on the vertical limbs of the transformer yoke at the horizontal mid-plane of the vacuum chamber, as illustrated in figure 1. There are, in all, three pairs of fission chambers, each pair comprising one ^{235}U fission chamber (and associated polyethylene moderator) and one ^{238}U fission chamber. The two types of chamber differ in neutron detection efficiency by a factor of 10^4. Through the employment of both pulse counting and current sampling, each chamber can operate usefully over a range of seven decades. By combining the two types of chamber, a total span of ten decades can be covered, from 10^{10} n/s to 10^{20} n/s. The response of the fission chambers is expected to be accurately linear but this has to be proven in practice. Thus, absolute calibrations should be performed for a range of intensities to an accuracy of 10% or better.

The most obvious method of calibrating the fission chambers is by taking a (point) neutron source into the vacuum vessel and moving it through a large number of positions so as to map out the response to be expected for an extended plasma. Ideally, to simulate the response to neutrons from a deuterium plasma, a 2.5 MeV neutron tube source would be used. Such a source has been used to good effect at the TFTR device in Princeton, U.S.A. [2]; unfortunately, such sources are expensive, are somewhat complicated for operation inside a tokamak, need careful characterization of the directional emission of the neutrons, do not give very accurate results (i.e. not better than 15%) and only operate at a very low level of equivalent neutron emission strengths.

More frequently, a ^{252}Cf radioisotope neutron source is substituted. It has been found, at TFTR [3,4] and in early work at JET [5], that the ^{252}Cf source adequately mimics the monoenergetic 2.5 MeV fusion neutrons. This finding is a result of the design of the ^{235}U fission chamber/moderator system which offers a nearly flat response for neutrons in the energy range from a few eV to 20 MeV [1]. Unfortunately, more recent experience at JET has shown [6] that the ^{252}Cf neutrons are being disproportionately moderated and absorbed, relative to 2.5 MeV neutrons, by the massive diagnostic equipment now interposed between the fission chambers and the diagnostic ports which constitute the main leakage path for plasma neutrons on their journey to the fission chambers. Thus, at JET, we can no longer rely on the use of a ^{252}Cf source for an accurate calibration.

Fortunately, it was always planned for the calibration to be obtained by the

application of activation techniques. To this end, a comprehensive pneumatic transfer system has been installed on the tokamak for the movement of samples between suitable irradiation positions close to the plasma and the remote nuclear instrumentation bay where the induced radioactivity is to be assayed.

A considerable effort has been devoted to performing the neutron transport calculations [7-9] needed to relate the neutron fluence at the irradiation position to the total yield of neutrons from the plasma. Early work with the activation system [10] concentrated on measuring the ratio of the yield of 14 MeV neutrons from the burnup of 1.0 MeV tritons (themselves produced in one branch of the d-d fusion reaction) to the 2.5 MeV neutrons produced in the other branch. The 14 MeV neutron fluence was measured with the $^{63}Cu(n,2n)^{62}Cu$ reaction, for which the reaction cross-section is known to an accuracy of about 4%. Activation measurements were also made to obtain the 2.5 MeV neutron emission [9,11] but, for the burnup study, the 2.5 MeV neutron emission was obtained from the fission chambers, calibrated using the in-vessel ^{252}Cf neutron source. This was considered more accurate than the use of the activation technique because there was, at that time, no suitable activation reaction available for use with 2.5 MeV neutrons which offered properties comparable to those of the $^{63}Cu(n,2n)^{62}Cu$ reaction. However, the recent commissioning of two delayed-neutron counting chambers [12] at JET now permits the use of ^{238}U samples, offering effective half-lives of less than 1 minute and for which the fission reaction cross-sections are known to about ±3%. Since the absolute efficiency of the delayed neutron chambers can be accurately determined in terms of ^{238}U fission events, the delayed neutron technique is capable of measuring neutron fluences to a few percent accuracy [13]. As will be shown, the neutron transport calculations have matured to the point where they are probably reliable to ± 5%. Thus, we are now in a position routinely to measure 2.5 MeV neutron yields of over 10^{14} neutrons to an absolute accuracy of better than ± 6%; henceforth, the triton burnup will be most reliably determined from the ratio of two activation measurements.

The present work, reporting experiments performed during the 1989 operating campaign, represents a significant correction to our earlier studies [8-10], an extension of experimental technique and an improvement in accuracy. Much relevant detail is provided in the previous publications and will not be repeated here. The remainder of this paper is organized as follows. In section 2, the activation analysis facility is described, with particular emphasis on the delayed-neutron counting method. In section 3, the neutron transport calculations are discussed and the deficiency in the original computer model of the tokamak is explained. The recent experimental results are presented in

section 4, their accuracy is evaluated in section 5 and, finally, in section 6, the status of results published earlier is assessed.

2. THE ACTIVATION ANALYSIS FACILITY

In principle, the mechanics of activating a suitable sample and, subsequently, determining the amount of activity produced are of extreme simplicity. The sample merely has to be placed at a suitable point in the radiation field for an appropriate duration before removal to a well-shielded analysis station for assay. Unfortunately, access to a large tokamak like JET is just as restrictive as to a fission reactor and the samples have to be moved between irradiation positions and analysis stations by means of a pneumatic transport system. Analysis of the samples is straightforward, either gamma radiation or delayed neutrons being detected; as the latter technique is novel for the fusion community, it will be described in some detail.

2.1 Choice Of Irradiation Positions

In order to obtain estimates of the total neutron yield without requiring prior information concerning the precise position of the plasma within the vacuum vessel, it was decided to establish positions inboard and outboard of the expected major radius; at each radial position there is a pair of vertical positions, one above and the other below the horizontal mid-plane of the machine. By averaging results obtained from the vertical pairs, a value for the yield independent of small vertical displacements of the plasma can be obtained. Likewise, by comparing inboard and outboard measurements, the radial position of the plasma can be estimated. However, for this purpose it is necessary to have recourse to detailed neutron transport calculations (see below). Fortuitously, it turns out that the outboard irradiation position is very little affected by radial displacements of the plasma; contrariwise, the inboard measurements are quite sensitive to radial position. So far, four irradiation positions have been defined. In fact, eight were originally provided so that potential toroidal asymmetries in neutron emission could be investigated (related, perhaps, to beam injector boxes or even ICRF heating antennas). Viewed from above, the inboard positions lie in a plane containing the (vertical) axis of symmetry of the tokamak; the outboard positions lie in a similar plane, almost orthogonal to the first (see fig.1). In order to simplify the neutron transport problems as much as possible, these irradiation positions are situated close to, but just outside, the double-walled vacuum vessel. They lie, therefore, in the interspace between the vessel and the toroidal field coils with their concrete-filled cast iron support structure.

It was expected that the portion of the tokamak of relevance for the neutron transport problem could be accurately modelled. However, this task has turned out to be more difficult than anticipated and a further two, more appropriately situated, irradiation ends have been installed, as described below. A drawing of a vertical section through one of the outboard irradiation ends is shown in fig. 2.

As no measurable toroidal effects have been identified, it will be clear that the neutron yield from a discharge can be obtained most conveniently from either of the two vertical pairs of outboard irradiation ends; measurement of the radial position of the plasma requires the inboard irradiation ends to be used also. In practice, the position of the plasma is obtained directly from the neutron emission profile diagnostic [14]. Thus, simultaneous use of inboard and outboard irradiation ends is mostly of value as a test of the accuracy of the neutron transport calculations.

In addition to the 8 irradiation positions outside the vacuum vessel, another pair of irradiation positions has recently been established inside the vacuum vessel. As usual, they form a vertical pair, with radial position intermediate between the older inboard and outboard positions; only the lower of these has so far been commissioned. These new inside irradiation ends were considered necessary because future plans for JET involve provision of substantial saddle coils close to the established irradiation positions, thereby severely restricting the accuracy with which the neutron transport calculations can be made. The new irradiation positions are not to be so shielded. Being inside the vessel, they have to be water cooled to prevent the melting of polyethylene capsules. One benefit accompanying these inside positions is the possibility of experimentally determining the attenuation to neutrons offered by the vacuum vessel. It was through comparison of this measurement with code predictions that a major source of modelling error was uncovered, namely, the neglect of the supporting structure separating the inner and outer walls of the vacuum vessel.

2.2 The Pneumatic Transport System

The samples are fitted into polyethylene capsules which are moved between a capsule loader, the irradiation positions, the various detectors and a capsule dump by means of a pneumatic transport system. The heart of the system is a 20-position carousel, which serves both to route the capsules as required and as a holding station for capsules awaiting irradiation or analysis. All transfers involve the carousel either as a sending or receiving end. Each

station (irradiation end, detector, etc) is controlled by a single plug-in electronics module which takes care of all pneumatic valve operations. The 20-module control unit is connected to a Norsk Data computer through which the entire system is driven with the aid of a colour video screen and associated touch-panel. Certain operations, once defined, can be repeated automatically for succeeding discharges until disabled.

2.3 The Delayed-Neutron Measurement System

If the material selected to be irradiated is fissionable (principally ^{232}Th, ^{235}U and ^{238}U), then a wide variety of radioactive fission products will be generated, including some which decay by beta-emission with half-lives of up to a few minutes to nuclides that emit neutrons. These beta-delayed neutrons can easily be detected by moderation and subsequent capture in, for example, a cluster of ^{3}He proportional counters. There are several beta emitters to be considered, with half-lives ranging up to one or two minutes. Conventionally, the neutron emission is represented by six groups, each characterized by a fractional yield, half-life and energy distribution. Whilst all fission events are accompanied by neutron emission, typically 2 to 3 neutrons per fission, approximately only 1 to 2% of these neutrons are delayed, the remainder being emitted promptly. For 2.5 MeV neutron induced fission, the total delayed neutron yields, the relative yields of the six half-life branches and their half-lives are all known with respectable accuracy [15]. However, as will be shown below, the degree of accuracy is not an issue for the present application.

Two identical delayed-neutron counting assemblies have been designed and built for use at JET [12]. Each consists of a polyethylene moderator in which is embedded a detector end of the transport system, to which a capsule can be transferred after irradiation. Six ^{3}He proportional counters surround the detector end, forming a hexagonal array. This assembly is enclosed within a cadmium envelope, beyond which is more moderator within a further cadmium envelope. This design ensures that the proportional counters are entirely insensitive to neutrons incident on the detector assembly through the external sides; in particular, there is no measurable cross-talk between the two assemblies.

Both delayed neutron counters have been extensively tested and calibrated using another capsule transfer system installed at the Belgian CEN/SCK BR-1 research reactor, using the Cavity Fission Spectrum Standard Neutron Field. All measurements were related to a National Bureau of Standards fission

chamber, which detects fission events with nearly 100% efficiency for foils that are thin compared with the range of fission fragments. Since the mass of fissionable material in the chamber is known, and the mass contained in the capsules is accurately measured, the number of fission events in the sample is easily determined for each irradiation. The capsules were irradiated, transported to the detectors and counted according to the same time sequence used at JET. For an assumed set of fractional neutron yields and half-life data, the measurement determines the neutron detection efficiency of the assembly. This was found to be (14.6 ± 0.28)% for ^{238}U. Different timing scenarios were tried and the same detector efficiency was found for all cases. Provided the same fractional yield and half-life data are used in the analysis of JET data, then this efficiency of 14.6% will be appropriate for the present application even if the assumed data are subsequently found to be moderately unreliable. With the efficiency so determined, the neutron yield in a JET discharge can be found using response coefficients for the irradiation position as determined by neutron transport calculations, which take into account the energy-dependent fission cross-sections.

The time sequence for a typical JET discharge (see fig 3) is as follows. The samples are positioned in the irradiation ends well before the discharge is initiated and are not removed until at least 5 seconds after the discharge has terminated. The delayed neutron counters are sampled at 20 msec intervals, starting at a well-defined moment in the JET timing sequence. The transfer time for the 150 metre journey via the carousel is 15 secs. The arrival of each capsule in the detector assembly is indicated by the sudden detection of neutrons. The various timings are important for the data analysis; in particular, the time-dependence of the neutron emission during the discharge as recorded by the fission chambers is also utilized. Since the cooling time is generally 20 to 30 seconds, the emission history is not of importance for short duration discharges. However, discharges with durations of up to 30 seconds have been run and, for these, the time history is vital.

Various tests of the correct performance of the counter assemblies are routinely made. Each proportional counter is provided with a separate signal processing chain, with two signal amplitude discrimination levels set so that the counting rate ratio is approximately 1.05. Any alteration in this ratio would indicate an electronics fault. Background count-rates are also recorded before capsule arrival; any significant background levels have so far been attributable to bursts of electrical noise from the proportional counters. Noisy counters have to be replaced as there seems to be no cure. Tests with a standard ^{241}Am-Be neutron source show that the overall efficiencies of the two

delayed neutron counters have not altered by as much as 1% since their tests at the BR1 reactor, over 3 years ago.

The delayed neutron counting system has three important features: (i) the absolute accuracy of the fluence measurement is determined mainly by the precision with which the fission reaction cross-sections are known, i.e. 3% in the case of ^{238}U; (ii) the entire system can operate automatically, the same capsules being used for every discharge since the time between discharges is generally 20 minutes or more (much longer than the decay time of the delayed neutron activity), and (iii) the data from the latching scalers are archived along with the other diagnostic data for the discharge.

2.4 The Gamma-Radiation Detection System

Simultaneously with the operation of the delayed-neutron counters, the transport system can also deliver capsules to a counter end positioned just above a shielded NaI scintillator or to one above a shielded high purity germanium diode (HPGe) for analysis without need for removal of the samples, provided these are sufficiently strongly activated. In practice, since the level of neutron emissions from JET is not very high (usually $<10^{16}$ n/discharge, i.e. fluences at the sample position are $<10^{10}$ n/cm^2) the samples destined for analysis with the HPGe detector are removed from their capsules and are placed directly on top of the detectors for optimum counting efficiency.

Both detectors are connected to a multi-channel analyzer (MCA), the HPGe detector signals being digitized in an ADC provided with a Westphal loss-free corrector module [16] for high count-rate applications. Control of the MCA is manual, with the data being stored on a 10 Mbyte disk controlled by an IBM personal computer whilst awaiting transfer to the mainframe computer.

2.5 Activation Sample Selection

The main limitation of the activation technique is the paucity of suitable nuclear reactions for use with 2.5 MeV neutrons. Ideally, the selected material should be monoisotopic, have an effective reaction threshold energy of about 1.5 MeV and a large and well-known cross-section leading to a daughter nuclide which decays by energetic gamma-emission (with high probability) with a half-life in excess of a few minutes but less than an hour. There are, of course, no such cases. Instead, the $^{115}In(n,n')^{115m}In$ reaction has become the tokamak standard, despite its low threshold energy, imprecisely known cross-sections and the possibility of interfering (γ,γ') reactions. The

$^{64}Zn(n,p)^{64}Cu$ reaction has a higher threshold energy, but the reaction cross-sections are even less well determined. Finally, the $^{58}Ni(n,p)^{58}Co$ reaction is suitable apart from the decay half-life of 71 days; this reaction can be used only with individual high yield discharges ($> 10^{16}$ neutrons) or a series of low yield discharges giving the same integrated yield.. This latter application will be discussed later.

The use of the $^{63}Cu(n,2n)^{62}Cu$ reaction for studying the 14 MeV neutron emission has been used previously at JET [10]. The experimental technique is well defined, but tedious. However, the $^{28}Si(n,p)^{28}Al$ reaction is preferred [17] for routine measurements as the 1.78 MeV gamma-ray from the decay of ^{28}Al is easily measured with a NaI detector, there are no interfering reactions and the 2.25 min half-life is sufficiently short that the data collection can be made part of the bulk data collection from the plasma discharge and the same sample can be re-used in successive discharges. Unfortunately, the $^{28}Si(n,p)^{28}Al$ reaction cross-section is not a dosimetry standard and cross-calibration against the $^{63}Cu(n,2n)^{62}Cu$ reaction is essential.

3. NEUTRON TRANSPORT CALCULATIONS

Measurements of induced radioactivity, obtained by studying gamma emission or delayed neutron emission, provide estimates of the neutron fluence at the irradiation position. In order to deduce the total neutron yield from the local fluence, recourse to neutron transport calculations is essential. Two different neutron transport codes (and their respective nuclear cross-section data sets) have been used to model JET. The first, FURNACE [7,8], is essentially a 2D ray-tracing code, with certain 3D attributes. FURNACE is ideal for sensitivity calculations since it provides precise results. Detailed features, such as the structure of the irradiation ends, cannot be modelled so the predictions may need to be supplemented with estimates of local shielding, depending on the circumstances. FURNACE is most useful for calculating the variation in the fluence at the irradiation position with plasma position or size. The second code, MCNP [18], is a standard 3D Monte Carlo code which should provide reliable estimates of neutron spectra and fluences but suffers from the customary lack of precision due to limited cpu time on the mainframe computer. For many situations the two codes provide results which are directly comparable; this possibility of comparing results provides a powerful means of uncovering programming mistakes and errors in data input and in the geometrical modelling of the tokamak.

3.1 FURNACE

The FURNACE code models only 1/16 of the tokamak, reflections on boundary surfaces enabling the complete 8-sector machine to be simulated. The diagnostic ports require 3D modelling and this is achieved in FURNACE in an approximate manner so that fluences should not be computed for points in the near vicinity of these ports. The FURNACE code has been documented in detail in relation to the JET calculations; reference [7] describes the basic code, and ref. [8] details the extensions for 3D effects.

3.2 MCNP

The MCNP code is used world-wide and has been thoroughly tested. Its application to the JET problem has been described in several papers [9-11]. The MCNP model of the JET machine is similar to that used in FURNACE, except that mirror symmetry about the median plane is assumed, so that only 1/32 of the tokamak is modelled; however, the effect of the irradiation ends can be included directly.

3.3 Comparison Of Code Predictions

The numerical results from the two neutron transport codes for deuterium plasmas of position and size typical of JET operation, as described in ref [7], and for source neutron energy spectra as detailed in ref [9] and specified later (section 4.3), are compared in Tables I to III for situations of increasing modelling severity, as described below. It will be seen that the agreement is very good. This satisfactory situation actually represents the conclusion of several year's experience, during which a number of errors in coding and modelling were discovered and corrected; even so, it will be shown that the results in Table III correspond to an unacceptably simplified modelling of the vacuum vessel.

3.3.1. Wall-Averaged Neutron Fluences And Nickel Activation

Table I tabulates the neutron spectra at the inner wall of the vacuum vessel, averaged over the entire wall surface. These results were required in support of experimental measurements [19] of the gamma dose-rate measured within the tokamak vacuum vessel after an extended period of operation during which the neutron yields were continuously monitored with the fission chambers.

Two models of the vacuum vessel are represented, the first, to be referred to

as the Old Model, corresponds to conditions applying between January 1985 and October 1988, when the centre column of the machine was covered with graphite tiles over a height of ± 1.00 m above the median plane. The original 16 discrete limiters were replaced with two belt limiters early in 1987; however, neither form of limiter was modelled at this time. Subsequently, and correctly represented in the New Model, the graphite tiling was extended to ± 1.36 m, extensive graphite protection of bellows sections and X-point dump plates was added and the two graphite belt limiters were now included. The most recent change, to beryllium belt limiters in August 1989, has no discernible effect on these calculations.

In Table I, the FURNACE and MCNP spectra are presented as averages over the inner surface of the vacuum vessel. The activation of the inconel wall is predominantly due to the $^{58}Ni(n,p)^{58}Co$ reaction; accordingly, the average activation coefficient, $<\sigma\phi>$, for this reaction is computed. Due to the large scoring area for the MCNP calculation, the statistical accuracy is excellent. The total neutron flux above 0.67 MeV is predicted by FURNACE to be about 10% greater than that predicted by MCNP, a discrepancy attributed to the use of different neutron transport data libraries by the two codes since the activation coefficients for the high energy threshold nickel reaction (which is sensitive mainly to unscattered neutrons) agree very closely. The library used by MCNP is the more up-to-date of the two. There is an overall systematic error arising from uncertainties in the activation cross-section data to be applied to both coefficients although, as will be shown later, this is probably much less than the 10% uncertainty indicated by the data evaluations.

The wall activation calculations were used to predict the gamma dose-rates inside the vessel after a lengthy period of operation. As described in ref 19, agreement at the 10% level between measurement and calculation was found. Subsequently, the need for a number of corrections has been appreciated but the agreement is unaffected as the corrections almost cancel.

3.3.2 Activation Of Sections Of Wall Taken From Small Circular Ports

At the same time as the in-vessel measurements were being made, some circular pieces of vacuum vessel were removed from the regions occupied by two of the small circular ports, very near the irradiation ends. The induced activity in each of these pieces of inconel was measured in the laboratory. The corresponding calculated neutron spectra are tabulated in Table II. As before, both FURNACE and MCNP spectra are computed for the vacuum interface with the wall.

The agreement between the two codes is within the statistical uncertainty associated with the MCNP computation. The ratio of computed ^{58}Co activities is 0.79 from FURNACE and 0.81 ± .05 from MCNP; each compares well with the measured value of 0.77 ± .02. The absolute level of the induced activity can be used to check the calibration of the fission chambers; it was found (after applying corrections too numerous to detail here) that the ratio of yields from the activation measurements to that from the fission chambers was 1.06 ± .12; the 15% uncertainty in the fission chamber calibration resulting from the in-vessel work has not been included. This comparison represents an average over several months operation and, therefore, over a wide variety of tokamak operating conditions (and neutron emission levels).

3.3.3 Calculations For The Use Of The Irradiation Ends

Since FURNACE cannot include the detailed structure of the irradiation ends, the two codes are best compared with the irradiation ends omitted. In Table III, the predicted activities for several materials are first compared (top section) for the Old Model with no irradiation ends. For FURNACE, the vessel was described as consisting of two 12-mm thick shells of inconel separated by a narrow interspace for CO_2 gas heating. For MCNP, the vessel was similar except that holes were left above the irradiation positions so as to simulate the actual geometry more accurately and (through a misreading of the engineering drawings) the inner section of the vessel was assumed to have an extra 8 mm. thickness. The agreement between the two sets of calculations is within the MCNP statistical uncertainties.

Because of the poor statistical limitations of MCNP calculations, the effects of the irradiation ends in these early calculations were evaluated by using the point-estimator technique for two runs in which the plasma, but not the surrounding structure, was modelled. The irradiation ends were included in only one of the runs and both were started with the same seed random number. The attenuation factor was found to be 0.874 ± .010, equivalent to that produced by a 6-mm thickness of inconel. The second set of calculations (centre section of Table III) compares results after simulating the irradiation ends by surrounding the irradiation position with a 6-mm shell of inconel. The MCNP calculations now adopt the 24 mm. total wall thickness for the whole vessel (the reduction in thickness making very little difference even to the inboard coefficients). The MCNP coefficients appear to be uniformly smaller than the FURNACE coefficients but, for reasons to be discussed below, this is believed to be of mostly statistical origin.

The lower section of Table III compares results obtained for the new geometry of the vessel. The first point to note is that the MCNP coefficients are apparently unaffected by the change in model, whereas the FURNACE coefficients for the new model of the vessel are reduced by about 9% ; the effect of the change to the model is more reliably calculated with FURNACE as this code is not bedevilled with statistical uncertainties. The agreement between the FURNACE and MCNP results is within the bounds expected from the statistical uncertainties associated with the MCNP results. However, it should be noted that the treatment of the effects of the irradiation ends is only approximate and is not be entirely self-consistent between the two codes.

The above comparison of computed coefficients is sufficient to demonstrate that FURNACE and MCNP calculations are in good agreement. This is a requirement, since they both use essentially the same model of the tokamak. Unfortunately, this model omits the structure within the double skin of the vacuum vessel. If the mass of the vessel (78 tonnes after subtracting the horizontal diagnostic ports) is divided by the $220m^2$ inner area, then it is seen that a homogenized vacuum vessel would be some 39mm thick, not 24mm. Homogenization is definitely not appropriate but the importance of including the support ribs is obvious. New calculations with improved modelling of the vacuum vessel have yet to be made. Instead, an effective thickness of the vessel can be determined experimentally by comparing results obtained with inside and outside irradiation ends.

Both FURNACE and MCNP codes have been used to obtain coefficients for the inside irradiation ends. Unfortunately, the irradiation ends have not yet been installed in their final positions since neither the saddle coils nor their protective limiters are yet in place. Consequently, the inside irradiation ends are partially shielded by the inner wall of the vacuum vessel where MCNP alone gives valid predictions. The variation of the activation coefficient for ^{238}U as a function of height above the horizontal mid plane is shown in fig. 4. The figure shows the MCNP results for the shielded region and the FURNACE results within the vessel; it also shows the experimental determination of the gradient of the response, which falls 16% in a further displacement of 5cm (from 194.5 to 199.5 cm). It should be noted that not only was it important to obtain accurate measurements of the actual sample position relative to the vacuum vessel walls but it was equally important to ensure that the MCNP modelling conforms precisely with these measurements.

After the calculations described above had been performed, it was realized

that the treatment of the effect of the irradiation end using the point-estimator technique was questionable, although its surrounding vacuum enclosure was included in the MCNP model. Accordingly, the irradiation end and the region occupied by the sample to be activated were modelled correctly so that track-length estimation could be used; the new coefficients were 3.5% higher than before for 2.5 MeV neutrons and 13.3% higher for 14 MeV neutrons. The cpu time required for the calculation was increased from about 20 minutes to about 20 hours. The coefficients obtained from this final calculation for a standard sample position of 194.5 cm. in the vacuum vessel (when at room temperature) are presented in Table IV.

4. EXPERIMENTAL RESULTS

The pneumatic transfer system has been used repeatedly for the activation of nickel, indium, zinc, copper and silicon samples for measurement of the gamma decay activities and of uranium and thorium for delayed neutron counting. The earlier studies of the neutron emission claimed only ± 20% accuracy for indium and zinc measurements (2.5 MeV neutron emission) and 10% for copper (14 MeV neutron emission) due to the large uncertainties associated with the neutron activation cross-section data and detector calibrations. As explained above, the delayed neutron technique is far more accurate. As will be shown, detailed cross-checking demonstrates satisfactory agreement between the delayed neutron and gamma activation measurements.

The activation measurements are weakly sensitive to the position of the plasma in the vessel and to the peaking factor of the radial profile of the neutron emission; data obtained from the neutron profile monitor permitted the necessary data adjustments to be made using the sensitivity study of Verschuur[8]. The necessary corrections for plasma position and shape were always less than 3%.

4.1 Treatment Of The Fission-Chamber Data

The calibration of the fission chambers was first performed in 1984 using a ^{252}Cf neutron source. This calibration has been transferred to the present time by repeated relative calibrations; in particular, the delayed neutron system was used to relate 1988 to 1989 operations. As a result of such manipulations, the original claim of ±10% accuracy should now be considered degraded to ±15% accuracy. This calibration nevertheless constitutes the reference for the work described here, i.e. the calibration factor from the 1984 calibration work is 1.00 ± 0.15.

A small correction to the fission chamber measurement of neutron yield is required to take into account the weak dependence on the plasma size and position [5]. This correction is obtained with the assistance of the neutron emission profile measured with the profile monitor [14]; the correction factor varies from 1.0 (for peaked profiles) to 1.15 (for broad profiles), with 1.08 being typical for normal discharges.

4.2 Treatment Of The Delayed-Neutron Data

The time-dependence of the neutron yield as obtained from the fission chambers is used to compute the variations of the fission event rate in the fission foils during the plasma discharge and the full history of delayed neutron emission is computed for each of the six decay half-lives using the absolute and relative yield data from Tuttle [15]. The calculated delayed neutron emission is then summed for the duration of the counting period and is used, together with the measured delayed neutron count and known neutron detection efficiency, to obtain the absolute neutron fluence at the capsule positions. Finally, the total neutron yield is obtained using the coefficients from Table IV, with the minor adjustments discussed below. In the treatment of the ^{238}U measurements, the (18%) contribution of the small ^{235}U contaminant (0.05%) has also to be taken into account; the coefficient for ^{235}U is determined empirically, using an enriched ^{235}U sample and the best available calibration for the fission chambers.

Whilst the delayed neutron counters were being calibrated in the ^{235}U fast fission neutron spectrum of the Mol BR1 reactor [12], it was found that the flux levels obtained from the ^{232}Th measurements were about 3.5% lower than those obtained from ^{235}U and ^{238}U. Accordingly, the fast fission integral cross-section for ^{232}Th measured earlier [20] at the BR1 facility was adjusted downwards by 3.5%. Adoption of this readjustment leads to essentially identical neutron yields being obtained at JET for ^{232}Th and ^{238}U samples.

It might appear to be sensible to use the measured fast fission integral cross-section data, σ_m, (listed in Table V) for all the 2.5 MeV dosimetry reactions involved in this work. The procedure would be to calculate first the Watt spectrum averaged cross-sections, σ_c. We assume that the fast fission spectrum is well represented for energies between 0.5 and 15 MeV by the Watt formulation [22]
$N(E) = \exp(-AE)\sinh(\sqrt{BE})$ with $A = 1.0123 \pm .011$, $B = 2.1893 \pm .1552$ and E in MeV. The Watt spectrum extends from very low energies up to 20 MeV and has

a mean energy of 2.016 MeV. The ratios σ_c/σ_m would then be used to adjust the spectrum averaged cross-sections used in the MCNP calculations. These ratios are listed in Table V. In practice, we have chosen to apply this adjustment technique only to those reactions for which the cross-sections can be considered to be relatively flat over the energy range of interest; this criterion identifies only the ^{232}Th, ^{238}U and ^{115}In reactions. The Watt averaged cross-sections for ^{58}Ni and ^{64}Zn are deemed inappropriate for the present application, since they represent averages over a range of several MeV near the maxima of the cross-sections, whereas the 2.5 MeV fusion neutrons lie in the sharply-rising portions of the excitation functions where reliable point cross-section data are needed. The Watt averaged data are clearly irrelevant with respect to the high threshold energy ^{28}Si and ^{63}Cu reactions. The cross-sections for the reactions of interest are plotted in fig.5, together with the Watt fast fission neutron energy spectrum and the Gaussian representing the 2.5 MeV neutrons from d-d fusion reactions.

To avoid the possibility of confusion, the choice of reaction cross-section data for the activation coefficients is reiterated. The basic point cross-section data are derived from the DOSCROS84 library [25]; however, data for ^{115}In and ^{232}Th are normalized to ^{238}U using the fast fission spectrum measurements. For neutron energies near 2.0 MeV, the relative errors for these three materials will be those of the integral measurements but their overall normalization error will be that associated with the point cross-sections for ^{238}U.

4.3 Treatment Of The Gamma-Emission Data

The calibration of the HPGe detector used for the gamma-ray measurements is straightforward in principle, using standard sources. However, because the samples were only weakly activated, they were placed directly on the detector window for optimum counting efficiency. In general, this is an undesirable practice because of sum-coincidence effects. Separate measurements with samples strongly activated in a 14 MeV neutron flux from a particle accelerator were used to cross-calibrate against the standard sources at the 10 cm distance. In this manner, the HPGe detector could be calibrated to an accuracy of ± 3% (1σ). The resulting detector efficiencies, including correction for self-absorption effects, are given in Table VI.

The samples typically weighed 15 g and, except for the silicon sample, took the form of four discs, 1.8 cm. dia., which were spread out on the top of the HPGe detector for analysis. Because the diode is not accurately positioned

within the cryostat, it is important that the samples be placed precisely on defined areas. Since the activities induced in copper and zinc decay by positron emission, it is good practice to place unirradiated discs on top of the irradiated discs during analysis to trap escaping positrons. Actually, this was not done during the analysis of actual discharges. Instead, separate tests were performed with accelerator-irradiated samples at a later time; the corrections to be applied for this oversight were found to be 3±1% for zinc (mean positron energy of 0.28 MeV) and 5±1% for copper (mean positron energy of 1.32 MeV). The silicon sample was in the form of a powder and was assayed using the NaI scintillation counter without removal from the capsule or counter end.

4.3.1 2.5 MeV Neutron Activation

The 2.5 MeV neutron activation measurements have to be corrected for the 14 MeV neutron contributions; this is easily achieved by using the MCNP coefficients for the two energies together with the 14 MeV fluences determined using the $^{63}Cu(n,2n)^{62}Cu$ and $^{28}Si(n,p)^{28}Al$ reactions. The magnitudes of the 14 MeV contributions for the various activation materials are indicated in Table VII, using the 14 MeV/2.5 MeV yield ratio of 1.5% that is typical in JET discharges for the purpose of illustration.

The neutron energy spectrum due to the d-d fusion reactions used for the calculations of the coefficients quoted in Tables III and IV are represented by a gaussian with a mean energy of 2.51 MeV and a broadening appropriate to a plasma temperature of 20 keV, as appropriate for situations in which the neutron emission is dominated by 80 keV D^0-beam heating [21]. The 56 keV upward energy shift is a secondary consequence of the finite reaction energy of the deuterons that give rise to the neutron emission.

When ICRF heating and D^0-beam heating are combined, there is a possibility that RF-acceleration processes will give rise to a deuteron population with a strong high energy tail; these energetic deuterons undergo fusion reactions with bulk plasma deuterons (and nuclear reactions with beryllium impurity ions, now that beryllium is being used for the belt limiter) with the result that neutrons of over 5 MeV energy can be produced. The fact that the $^{28}Si(n,p)^{28}Al$ reaction, with a reaction threshold of about 5 MeV, was routinely monitored to measure the 14 MeV neutron yield allows us to conclude that the RF-induced contribution of neutrons above 5 MeV was never more than 10% of the 14 MeV yield, or 0.1% of the total yield, for combined heating discharges. However, this does not imply that the excess yield between 2.5 and 5 MeV was

also negligible. Fortunately, measurements of the neutron energy spectrum are made for all JET discharges using, inter alia, a high resolution neutron time-of-flight spectrometer [23] which covers the range 2 to 4 MeV. Ideally, full neutron transport calculations should be performed using these measured energy spectra. This is quite impractical, and also unnecessary as the extra high-energy component rarely exceeds 20%. Instead, these spectra were used to calculate effective reaction cross-sections for comparison with those computed for the energy spectrum adopted for the MCNP calculations. Appropriate correction factors were thus generated individually for the combined heating discharges. These corrections are only significant for the ^{58}Ni and ^{64}Zn measurements, the flat cross-sections for the ^{232}Th, ^{238}U and ^{115}In reactions ensuring that their spectrum-dependent effects are small.

The d-d neutron yields obtained with these activation techniques are presented in Table VIII, where they are expressed in terms of the fission chamber yields. The gamma-decay measurements were all obtained using the new (Octant 3, lower) irradiation end. The delayed neutron measurements were necessarily obtained using a different irradiation end but they could be converted as appropriate for the new irradiation end because the relative responses for all the irradiation ends have been carefully determined using the fission chambers for reference purposes, as reported in Table IX.

The four activation measurements agree within their associated uncertainties. The indium and the delayed neutron measurements are in excellent agreement, as expected since their cross-section data have been adjusted to fit the integral cross-section measurements and their detector efficiencies have been determined to better than 3% accuracy. The nickel result is also in agreement with the first two, despite the absolute error on the cross-section data of at least ±10%. The zinc result is about 24% high, a large discrepancy considering the uncertainty in the cross-section data (±12%). The definitive calibration factor is taken to be that provided by the delayed neutron measurement because the associated uncertainties are all estimated to be smaller than those of the gamma-decay measurements; the main role for the latter has been to confirm that no unexpected systematic errors of significance are associated with the delayed neutron technique.

4.3.2 14 MeV Neutron Activation.

The study of the time-dependent emission of 14 MeV neutrons from triton burnup provides important information concerning the behaviour of fast particles in fusion plasmas. At JET, such measurements are obtained using a silicon diode

[24], which exploits the $^{28}Si(n,p)^{28}Al$ and $^{28}Si(n,\alpha)^{25}Mg$ reactions. A major concern with this diagnostic is that high-energy γ-rays and pulse pile-up due to inelastic scattering of 2.5 MeV neutrons in silicon will contaminate the signal due to 14 MeV neutrons. This possibility can be tested using the $^{28}Si(n,p)^{28}Al$ activation reaction, with samples irradiated with the capsule transfer system. Comparison of activation and pulse-integrated data from the diode shows close proportionality for all but the highest intensity discharges when beam-heating is used. For RF-only discharges, the silicon activation measurement frequently become disproportionately large. This is because the presence of high-energy neutrons associated with the RF affects the activation measurement, with its 5 MeV threshold, more than the diode, which is operated with a bias setting equivalent to about 8 MeV.

Since the $^{28}Si(n,p)^{28}Al$ cross-sections are not well known, it was not appropriate to use this reaction to obtain the absolute calibration for the diode. Its primary applications were to explore the relative responses to 14 MeV neutrons in different irradiation ends (Table IX) and to test the linearity of the silicon diode response to neutron intensity.

A number of discharges were studied using the copper reaction and a calibration factor for the silicon diode of $(2.42 \pm 0.13) \times 10^{10}$ 14 MeV neutrons per recorded event in the diode was obtained. The fractional burnup of the tritons emitted in d-d reactions depends sensitively on plasma conditions and must be studied using a time-dependent code; the results of the measurements obtained during the most recent operational campaign will be reported separately.

Examination of the results presented in Table IX shows that the responses for the four outboard irradiation ends are equal, within the measurement accuracy of $\pm$ 2%, irrespective of reaction employed. For the inboard irradiation ends, however, the copper result deviates significantly from the average. The inference is that equal relative responses for all reactions are obtained provided the reaction threshold is well below the neutron energy of interest. However, when the reaction threshold approaches the neutron energy, the relative responses are likely to become specific to the reaction under study (e.g. zinc for 2.5 MeV neutrons and copper for 14 MeV neutrons). In the present work, this effect is only significant for the inboard irradiation end. The same observation has been made before, during the course of multi-foil measurements [11], and is the reason for preferring the outboard positions for such work.

Once the calibration factor for the diode had been obtained from the copper activation measurements, an effective activation coefficient could be obtained experimentally for silicon [17]; this value was found to be $(2.0 \pm 0.2) \times 10^{-31}$, whereas the value obtained from the neutron transport calculations is 1.57×10^{-31}. The difference between these two figures is larger than expected on the basis of the known experimental errors. Since the copper reaction has a relatively high reaction threshold, it is quite sensitive to the neutron energy spectrum adopted as input to the MCNP calculations; a gaussian spectrum centred at 14.13 MeV and with fwhm of 1.69 MeV has been chosen as being representative of the emission from 1.0 MeV tritons slowing down in typical JET plasmas. It is most unlikely that this spectrum could be sufficiently in error to explain the activation coefficient discrepancy for silicon.

5. ASSESSMENT OF UNCERTAINTIES

The main contributions to the overall uncertainty of the neutron yield measurements are listed in Table X. Effects which introduce minor corrections, of less than 2%, are considered to be sufficiently well determined that the associated uncertainties can be neglected. The small number of items listed in the table is justified as follows.

5.1 Fission Chamber Yields

It is assumed that only well-behaved discharges will be studied for calibration purposes. This excludes low-density ohmic discharges, in which significant run-away electron currents are formed, and disruptive discharges in general; both classes produce photoneutrons which are efficiently detected by the fission chambers but not by the high-threshold activation reactions. ICRF heating is also potentially troublesome, as explained above, so ICRF-only heated discharges with high RF power to electron density ratios are ignored. For preference, combined RF and NBI heated discharges would also be avoided but this is not practical since most JET discharges employ combined heating.

Apart from sensible selection of discharges to be examined, the only other precaution is to apply the geometrical correction factor for finite plasma size and deviations of position from the centre of the vessel. The algorithm for determining the correction factor (typically, close to 1.08) is not very accurate but is applied consistently and any error can be considered to be absorbed into the overall calibration factor.

There is a statistical error to be associated with the fission chamber yields. This is trivially determined when operating in count mode. However, when in current mode the instrumentation integrates with a short time-constant and samples the voltage signal at 10 ms intervals; the resulting fluctuation about the true yield should never exceed ± 0.61% (i.e. a ratio between two chambers of ± 0.86%).

5.2 Delayed Neutrons

The detection efficiency is slightly different for ^{232}Th and ^{238}U due to differences in the mean energies of their delayed neutron emissions; the overall uncertainties are ± 1.0% random and ± 2.4% systematic for ^{232}Th and ± 0.9% random and ± 1.9% systematic for ^{238}U [12]. The systematic uncertainties derive from the integral cross-section data and so should be kept separate.

The uncertainties associated with the dosimetry library data have been partially side-stepped through the use of the fast fission integral cross-section measurements. This is only possible because the fission reactions offer practically flat cross-sections over the energy range of interest. This leaves only the point cross-sections for ^{238}U to be considered. One might expect the experimental uncertainties for the integral cross-sections for both ^{232}Th and ^{238}U and reactions to be taken into account. However, it has been found in earlier measurements that the neutron yields obtained with these two reactions are practically identical; in effect, the ^{232}Th reaction has been adjusted to give the same result as the ^{238}U reaction. Consequently, only the uncertainties associated with the point cross-section data for ^{238}U need be retained. No ^{238}U measurement is recorded in Table IX for Octant 3 because the need for the measurement with the enriched ^{235}U sample, necessary to correct for the small quantity of ^{235}U in depleted uranium, was overlooked.

The linearity of the fission chamber response as a function of neutron emission strength is shown in fig 6, where the ratio of the delayed neutron yield to the fission chamber yield is plotted against neutron yield (an approximate measure of intensity for the discharges studied). Linear regression analysis returns a line with zero gradient. The standard deviation for individual points is 3.0%; this is due mainly to the poor statistics of the delayed neutron counting method, with 300 counts per discharge being obtained for the lowest yield discharges (10^{14} neutrons), increasing to 30,000 for the highest yields. In addition, no account has been taken of possible vertical displacements of the plasma. When the averages of yields for both irradiation ends of a vertical pair are taken, the standard deviation reduces to 2.4%, an improve-

ment partially attributable to the discharges now being restricted to yields in excess of 10^{15} neutrons (i.e. with, typically, 10^4 delayed neutron counts). After subtracting the combined statistical errors of the delayed neutron and fission chamber measurements, there is a 2.0% residual of undetermined origin.

The statistical accuracy of the mean value of the ratio of two neutron yield estimates naturally improves with the neutron yield and with the number of measurements. Thus, the accuracy of the averaged ratio of delayed neutron to fission chamber yields was better for Octant 2 (± 0.5%) than for Octant 3 (± 1.5%), because the use of the latter position coincided with a period of low yield discharges, and was rather poor (± 4%) for the indium activation to fission chamber yield ratio measurements due to the low number of discharges studied with the activation technique.

5.3 Gamma-decay Measurements

Although the integral cross-section for indium has also been adjusted to that for ^{238}U, two different measurement techniques are involved and the uncertainties for both must be retained. Note that if the indium dosimetry cross-sections were to be used directly, the uncertainty associated with the library would have to be taken into account. The uncertainties in the 2.5 MeV cross-sections for all reactions of present interest are noted in Table X.

5.4 Transport Calculations

The response coefficients derived for the sample height of 194.5 cm. are the result of an averaging process for different heights, using MCNP and FURNACE calculations as well as experimental measurements of the fluence gradient. In these circumstances, it is not appropriate to adopt the full ± 3% statistical uncertainty of the MCNP calculations as being relevant for the merged result. Instead, the statistical uncertainties can be understood to be incorporated in the systematic error.

The assignment of a systematic error to the transport calculations should be the result of a detailed sensitivity analysis, taking account of simplifications in geometrical modelling, neutron transport cross-sections, source description, etc. Lacking such an analysis, an intuitive approach must be adopted. Fortunately, the coefficients are not highly sensitive to minor details of the model adopted for the vacuum vessel; indeed, even such a major omission as the structure separating the two shells led to an error of only about 30% for the irradiation positions outside the vacuum vessel. The effect

of increasing the vessel thickness (not yet done) on the coefficient for the inside position, situated in a port through the vessel, is expected to be negligible. For this position, the combined effects of the irradiation end structure and that of its vacuum enclosure (or thimble) is an attenuation by nearly 25%. Thus, accurate modelling of the region close to the irradiated sample is most important. The assumed systematic uncertainty of ± 5% is a generous allowance for the approximations made in performing this task.

The uncertainty attributable to the transport cross-sections is probably small since they are generally known to good precision and enter mainly through the downscattered flux contribution to the activation in the new irradiation position. The good agreement between FURNACE and MCNP, which use different transport cross-section libraries, attests to this insensitivity.

5.5 Accuracy of Final Results

The accuracy of the comparison of neutron fluences measured by delayed neutron and indium activation techniques is ± 6%. The two measurements actually agree to within 1%. The excellent agreement obtained with the nickel measurements validates the use of the DOSCROS84 library for the vessel activation studies. However, the zinc measurements indicate that the library data should be raised by 23% if agreement is to be obtained with the other reactions.

The accuracy of the calibration factor of 1.12 found for the fission chambers is ± 6.1%, obtained by averaging the delayed neutron and indium activation results. It should be recognized that this calibration refers to the total neutron emission from the plasma, i.e. it gives the sum of the 2.5 and 14 MeV emissions.

Finally, the uncertainty in the yield of 14 MeV neutrons is about 8%; this is likely to be the best that can be achieved for d-t plasmas. The uncertainty in the 14 MeV to 2.5 MeV neutron yield ratio is found to be ± 6%, after discounting the systematic uncertainties in the two activation coefficients on the grounds that they are strongly correlated but including the MCNP statistical error in the coefficient for copper.

6. DISCUSSION

The measurements presented in Table VIII, together with the activation coefficients listed in Table IV, show that the coefficients adopted in previous publications were all significantly in error. For ease of comparison, the

best experimental values resulting from the present work are presented at the foot of Table IX, where it has been assumed that the coefficients for indium can be obtained by scaling from those for thorium or uranium. However, this scaling might not be valid for the high reaction threshold of zinc so the coefficients for this material are quoted within parentheses.

The previous applications of the activation technique to the calibration of the fission chambers [9] and the determination of the fractional triton burnup [10] both referred to the coefficients listed in the top section of Table III. The calibration factor obtained by averaging the inboard and outboard irradiation end measurements was 1.08 from the use of indium and 0.87 from the use of zinc. On substitution of the activation coefficients from Table IX (scaled to the Old Geometry), the indium result converts to 1.57; the zinc result converts to 1.37. Later work [10] included the attenuating effect of the irradiation ends (centre section of Table III). The calibrations obtained with the outboard ends were 0.86 and 1.13 from indium and zinc, respectively, and convert to new calibrations of 1.13 and 1.39, where the New Geometry is now assumed to be appropriate since the belt limiters were installed when these measurements were made (although the Old Geometry coefficients were used at the time) and FURNACE calculations indicate that the outboard positions were mainly affected by the belt limiters. The two experiments [9] and [10] are clearly inconsistent; the first indium measurement is now regarded as being unaccountably high. The second indium measurement and the two zinc measurements are essentially identical with the present values of 1.14 and 1.39, respectively; such excellent agreement must be largely coincidental because the accuracy of the earlier measurements relative to the present work is unlikely to be better than ±10% when contributions from the separate measurements of detector efficiencies and the uncertainties concerning the modelling of the vacuum vessel are taken into account.

The re-evaluation of earlier work, given above, together with the fission chamber calibration derived from the measurement of activity induced in the vacuum vessel wall (section 3.3.2), are consistent with a calibration factor that has not changed since the beginning of 1986. This implies that the original in-vessel calibration obtained in January 1984 was also low by just one standard deviation. Further in-vessel calibration work in March 1989 produced confusing results; with the wisdom of hindsight, these later measurements can be re-assessed to give a calibration factor in the range 1.10 to 1.20, in fair agreement with present result.

The triton burnup measurements were reported [10] as being only 75% of the

classically expected value. Knowing that the outboard positions were employed, the average burnup can now be converted to 89% of the classical value, after taking account of the new fission chamber calibration factor. The time-resolved triton burnup measurements of ref [24] implied a fractional burnup of 17% higher than the values derived from the activation measurements; on the present understanding, this converts to a fractional burnup of 1.04 times the classical value. There are appreciable uncertainties (± 20%) to be associated with the classical calculations due to the imprecise knowledge of the basic plasma parameters.

7. CONCLUSIONS

This work has shown that the total yields of 2.5 MeV and 14 MeV neutrons from JET discharges can be made with an accuracy of 8% or better. The largest source of uncertainty lies with the neutron transport calculations, with the region closely surrounding the sample position meriting careful attention.

The delayed neutron technique has been assessed to be more accurate for determining the 2.5 MeV neutron yields than assessments of gamma-decay activity and is eminently more suitable for routine operations. Similarly, the $^{28}Si(n,p)^{28}Al$ reaction is suitable for routine measurements of 14 MeV neutron yields, but it must be calibrated in terms of the copper reaction. Further, care must be exercised when ICRF heating is employed.

With the wide range of techniques now available, it has been found possible to determine experimentally the activation coefficients for all irradiation positions relative to the new irradiation position, for which the neutron transport calculations should be particularly reliable since it is placed inside the vacuum vessel.

Finally, the present work has demonstrated that our previous calculations of the activation coefficients for the outside irradiation ends were significantly in error due to inappropriate modelling of the double skin of the vacuum vessel and that the results based upon them have to be revised.

REFERENCES

1. M.T.Swinhoe and O.N.Jarvis, "Calculation and Measurement of ^{235}U and ^{238}U Fission Counter Assembly Detection Efficiency", Nucl. Instrum. and Methods in Phys. Res. 221(1984)460.
2. E.B.Nieschmidt, A.C.England, H.W.Hendel, D.L.Hillis, J.A.Isaacson, L.P.Ku and F.Y.Tang, "Effects of Neutron Energy Spectrum on the Efficiency Calibration of Epithermal Neutron Detectors", Rev. Sci. Instrum. 56(1985)1084.
3. H.W.Hendel, D.L.Jassby, H.S.Bosch, C.W.Barnes, L.C.Johnson, T.J.Murphy, E.B.Nieschmidt, T.Saito, J.D.Strachan, G.D.Tait and K.M.Young, "TFTR Epithermal Neutron Detector System: Recalibration and Effect of Nonisotropic Neutron Emission", Rev. Sci. Instrum. 59(1988)1682.
4. L.P.Ku, H.W.Hendel and S.L.Liew, "Calculation of the Absolute Detection Efficiency of a Moderated ^{235}U Neutron Detector in the Tokamak Fusion Test Reactor", Nucl. Instrum. and Methods in Phys. Res., A280(1989)113.
5. O.N.Jarvis, J.Kallne, G.Sadler, P.van Belle, M.Hone, V.Merlo, E.W.Lees, M.T.Swinhoe, A.R.Talbot and B.H.Armitage, "Further Calibrations of the Time Resolved Neutron Yield Monitor (KN1)", JET-IR(85)06.
6. O.N.Jarvis, G.Sadler, P. van Belle and T.Elevant, "In-vessel calibration of the JET neutron monitors using a ^{252}Cf neutron source: difficulties experienced", Accepted for publication in Rev. Sci. Instrum.
7. K.A.Verschuur, "FURNACE, A Toroidal Geometry Neutronic Program System: Method Description and Users Manual", Netherlands Energy Research Foundation ECN-162 (1984).
8. K.A.Verschuur, "Neutron Transport Calculations in Support of Neutron Diagnostics at JET", Netherlands Energy Research Foundation, ECN-86-097 (1986).
9. M.Pillon, O.N.Jarvis, J.Kallne and M.Martone, "Calibration of Neutron Yield Activation Measurements at JET", Fusion Technology, 15(1989)1420.
10. J.Kallne, P.Batistoni, G.Gorini, G.B.Huxtable, M.Pillon, S.Podda and M.Rapisarda, "Triton Burnup Measurements in JET using A Neutron Activation Technique", Nuclear Fusion 28(1988)1291.
11. M.Pillon, O.N.Jarvis and S.Conroy, "Neutron Energy Spectrum Determination Near the Surface of the JET Vacuum Vessel using the Multifoil Activation Technique", JET-P(89)25.

12. P.D'hondt, S.de Leeuw, R.Menil and Y.Bortels, "Delayed Neutron Counting System for JET Plasma Neutron Yields Diagnostic", CEN/SCK No. 528007/510, (1986).
13. P. van Belle, O.N.Jarvis, G.Sadler, S.de Leeuw and P.D'Hondt, "Calibration of the JET neutron yield monitors using the delayed neutron counting technique", Accepted for publication in Rev. Sci. Instrum.
14. J.M.Adams, A.Cheetham, S.Conroy, G.Gorini, N.Gottardi, T.Iguchi, O.N.Jarvis, G.Sadler, P.Smeulders, N.Watkins and P. van Belle, "Radial Profiles of Neutron Emission from Ohmic Discharges in JET", Proc. 16th European Conf. on Controlled Fusion and Plasma Physics, Eur. Conf. Abstracts Vol.13B, Part I, (1989), p.63.
15. R.J.Tuttle, "Delayed-Neutron Data for Reactor-Physics Analysis", Nuclear Science and Engineering 56(1975)37.
16. G.P.Westphal, Nucl. Instrum. Meth. 146 (1977) 605.
17. G.Sadler, O.N.Jarvis and P. van Belle, "Use of the $^{28}Si(n,p)^{28}Al$ reaction for the measurement of 14 MeV neutrons from fusion plasmas", Accepted for publication in Rev. Sci. Instrum.
18. "MCNP - A General Purpose Monte-Carlo Code for Neutron and Photon Transport", LA-7396-M Rev. Version 2B, Los Alamos Monte Carlo Group, Los Alamos National Laboratory (1982).
19. O.N.Jarvis, G.Sadler, A.Avery and K.A.Verschuur, "Activation of the JET Vacuum Vessel; a Comparison of Calculated with Measured Gamma-Radiation Fluxes and Dose-Rates", JET-R(88)05.
20. D.M.Gilliam, J.A.Grundl, G.P.Lamaze, E.D.McGarry and F. Fabry, "Cross-Section Measurements in the ^{235}U Fission Spectrum Neutron Field", Proc. of the 5th ASTM-Euratom Symposium on Reactor Dosimetry, Geesthacht, F.R.G. Sept. 24-28, 1984, p.867.
21. P. van Belle and G.Sadler, "The Computation of Fusion Product Spectra from High Temperature Plasmas", in Basic and Advanced Fusion Plasma Diagnostic Techniques, (Varenna, 1986), EUR 10797 EN. Vol.III, p.767.
22. W.L.Zijp and J.H.Baard, "Nuclear Data Guide for Reactor Neutron Metrology", EUR 7164 EN (1981), p.148.
23. T.Elevant, D.Aronsson, P. van Belle, G.Grosshoeg, M.Hoek, M.Olsson and G.Sadler, "The JET Neutron Time-of-Flight Spectrometer", JET-P(89)76.
24. S.Conroy, O.N.Jarvis, G.Sadler and G.B.Huxtable, "Time-Resolved Measurements of Triton Burnup in JET Plasmas", Nuclear Fusion 28(1988)2127
25. W.L.Zijp, H.J.Nolthenius and G.C.H.M. Verhaag, "Cross-Section Library DOSCROS84 (in the SAND-II format)", Report ECN-160 (ECN, Petten, 1984).

Table I

FURNACE AND MCNP 2.5 MEV NEUTRON FLUXES
AVERAGED OVER THE SURFACE OF THE FIRST WALL

Group	Energy Boundaries Upper	Lower	Old Model FURNACE	Old Model MCNP	New Model FURNACE	New Model MCNP
17	3.01	2.72	3.0	2.9 ± 2.8%	2.3	2.3 ± 2.8%
18	2.72	2.47	33.6	32.3 ± 0.8%	27.1	26.7 ± 0.8%
19	2.47	2.23	45.3	44.2 ± 0.9%	36.9	36.5 ± 0.8%
20	2.23	2.02	18.4	18.7 ± 1.9%	16.7	17.4 ± 1.6%
21	2.02	1.83	7.5	6.9 ± 3.4%	10.3	9.4 ± 2.5%
22	1.83	1.65	4.8	4.3 ± 4.3%	8.2	7.6 ± 2.6%
23	1.65	1.50	4.3	3.9 ± 4.5%	7.0	6.3 ± 2.9%
24	1.50	1.35	5.0	4.6 ± 4.3%	6.7	6.1 ± 3.0%
25	1.35	1.22	5.4	4.7 ± 4.4%	6.4	6.1 ± 3.6%
26	1.22	1.11	8.3	5.7 ± 4.2%	8.0	6.1 ± 3.2%
27	1.11	1.00	9.4	8.1 ± 3.4%	8.3	7.4 ± 3.1%
28	1.00	0.91	9.6	7.4 ± 3.3%	8.3	6.1 ± 3.1%
29	0.91	0.82	10.4	8.7 ± 3.1%	8.7	7.2 ± 2.8%
30	0.82	0.74	10.5	9.0 ± 3.2%	8.8	7.5 ± 2.7%
31	0.74	0.67	9.4	8.5 ± 3.1%	8.0	6.9 ± 2.9%
			185.1	170.1 ± 0.6%	172.0	159.8 ± 0.6%
$\langle\sigma\phi\rangle$ values for ^{58}Ni(n,p)			9.8-32	9.5-32 ±1%	8.3-32	8.3-32 ±1%

The fluences are quoted in units of 10^{-4} neutrons/ m^2 per source neutron. The activation coefficients, $\langle\sigma\phi\rangle$, are quoted per source neutron and are to be interpreted as follows: 9.8-32 = 9.8×10^{-32}.

Table II

NEUTRON FLUENCES AT LOCATIONS FROM WHICH SMALL PIECES OF VACUUM VESSEL WERE SUBSEQUENTLY REMOVED FOR LABORATORY ANALYSIS.

Group	Energy Boundaries Upper	Lower	4C - Inboard FURNACE	4C - Inboard MCNP	6D - Outboard FURNACE	6D - Outboard MCNP
17	3.01	2.72	2.4	5.3 ± 15 %	3.1	7.0 ± 11 %
18	2.72	2.47	26.7	34.4 ± 8 %	34.5	41.3 ± 5 %
19	2.47	2.23	36.6	33.1 ± 8 %	46.9	41.2 ± 5 %
20	2.23	2.02	15.4	9.5 ± 14 %	19.2	11.5 ± 10 %
21	2.02	1.83	6.2	2.5 ± 32 %	7.5	4.1 ± 15 %
22	1.83	1.65	3.8	3.1 ± 26 %	4.9	3.3 ± 17 %
23	1.65	1.50	3.4	2.1 ± 34 %	4.4	3.0 ± 18 %
24	1.50	1.35	4.1	2.3 ± 30 %	5.2	5.4 ± 15 %
25	1.35	1.22	4.6	3.8 ± 30 %	5.6	5.6 ± 19 %
26	1.22	1.11	7.2	6.6 ± 24 %	8.9	5.7 ± 14 %
27	1.11	1.00	8.4	5.2 ± 20 %	10.1	10.1 ± 12 %
28	1.00	0.91	8.7	5.1 ± 22 %	10.3	9.5 ± 14 %
29	0.91	0.82	9.4	11.7 ± 15 %	11.0	10.2 ± 12 %
30	0.82	0.74	9.6	9.0 ± 15 %	11.1	9.1 ± 12 %
31	0.74	0.67	8.5	6.6 ± 22 %	10.0	8.2 ± 12 %
			155.0	140.3 ± 4 %	192.7	175.2 ± 3 %
$\langle\sigma\phi\rangle$ values for ^{58}Ni(n,p)			7.9-32	8.5-32 ±5%	10.0-32	10.5-32 ±5%

The fluences are quoted in units of 10^{-4} neutrons/ m^2 per source neutron and refer to the vacuum interface with the first wall. Location 6D corresponds to the Outboard Activation Position, but position 4C does not correspond to the Inboard Position.

The Old Model of the vacuum vessel has been used.

Table III

ACTIVATION COEFFICIENTS COMPUTED WITH FURNACE AND MCNP FOR THE OUTSIDE (INBOARD AND OUTBOARD) IRRADIATION ENDS (2.5 AND 14 MEV NEUTRONS)

OLD GEOMETRY (1987)

Reaction	FURNACE		MCNP		MCNP Statistics	
	Inboard	Outboard	Inboard	Outboard		
	No irradiation end corrections applied.		Excess 0.8 cm of wall inboard. Irradiation ends modelled for copper only.			
$^{64}Zn(n,p)$	1.06-32	1.56-32	1.04-32	1.58-32	10%	6%
$^{115}In(n,n')$	1.52-31	2.31-31	1.42-31	2.36-31	8%	5%
$^{232}Th(n,f)$	5.29-32	8.41-32				
$^{238}U(n,f)$	2.41-31	3.71-31				
$^{63}Cu(n,2n)$ -14 MeV			8.15-32	1.43-31	10%	6%
	Irradiation end correction factor of 0.874 applied.		Irradiation ends modelled for all materials.			
$^{64}Zn(n,p)$	0.93-32	1.36-32	0.73-32	1.12-32	6%	4%
$^{115}In(n,n')$	1.33-31	2.02-31	1.15-31	1.85-31	7%	4%
$^{232}Th(n,f)$	4.62-32	7.35-32	3.97-32	6.67-32	8%	5%
$^{238}U(n,f)$	2.11-31	3.24-31	1.80-31	3.00-31	8%	5%
$^{63}Cu(n,2n)$ - 14 MeV			1.10-31	1.41-31	10%	6%

NEW GEOMETRY (1989)

$^{58}Ni(n,p)$	2.63-32	4.12-32				
$^{64}Zn(n,p)$	0.79-32	1.22-32	0.65-32	1.06-32	5%	3%
$^{115}In(n,n')$	1.21-31	1.89-31	1.12-31	1.81-31	5%	3%
$^{232}Th(n,f)$	4.23-32	6.83-32	3.94-32	6.53-32	6%	3%
$^{238}U(n,f)$	1.94-31	3.04-31	1.78-31	2.92-31	6%	3%
$^{63}Cu(n,2n)$ - 14 MeV			9.58-32	1.40-31	5%	3%

Table IV

ACTIVATION COEFFICIENTS COMPUTED WITH MCNP FOR THE NEW (INSIDE) IRRADIATION ENDS: 2.5 MEV AND 14 MEV NEUTRONS.

Reaction	Activation Coefficients (per source neutron)					
	2.5 MeV			14 MeV		
	$\langle\sigma\phi\rangle$		error	$\langle\sigma\phi\rangle$		error
$^{28}Si(n,p)^{28}Al$				1.57E-31	±	3.0%
$^{58}Ni(n,p)^{58}Co$	7.38E-32	±	3.1%	2.90E-31	±	3.1%
$^{63}Cu(n,2n)^{62}Cu$				2.31E-31	±	2.9%
$^{64}Zn(n,p)^{64}Cu$	1.89E-32	±	3.3%	1.28E-31	±	2.9%
$^{115}In(n,n')^{115m}In$	2.92E-31	±	2.9%	0.88E-31	±	4.6%
$^{232}Th(n,f)$	1.05E-31	±	3.2%	2.23E-31	±	2.8%
$^{238}U(n,f)$	4.74E-31	±	3.2%	7.08E-31	±	2.8%
Fluence (n/cm^2)	1.77E-6	±	2.4%	6.92E-07	±	2.9%

N.B. The above coefficients include the attenuating effects of the irradiation ends. The vertical height above the horizontal midplane of the vacuum vessel, at room temperature, is taken to be 194.5 cm. The cross-section data are taken from the DOSCROS84 library [25]. The low energy cutoff for the neutron fluence is 0.302 MeV.

Table V

FAST FISSION INTEGRAL CROSS-SECTIONS AND WATT AVERAGED DOSCROS84 VALUES

Reaction	Experimental	$\frac{\text{Calculated DOSCROS84}}{\text{Experimental}}$
$^{58}Ni(n,p)^{58}Co$	111 ± 2.4%	0.934
$^{64}Zn(n,p)^{64}Cu$	30 ± 5.4%	1.191
$^{115}In(n,n')^{115m}In$	190 ± 2.1%	0.937
$^{232}Th(n,f)$	80 ± 2.4%	0.930
$^{235}U(n,f)$	1200 ± 1.9%	1.030
$^{238}U(n,f)$	312 ± 2.3%	0.971

The above experimental values are obtained from [20], except for ^{232}Th, which is a new measurement [12], and for ^{64}Zn, which is taken from ref. [25]. The Watt prescription for the ^{235}U fission neutron spectrum is that recommended in [22]. The cross-section data are taken from the DOSCROS84 library.

Table VI

ACTIVATION CHARACTERISTICS AND HPGE DETECTOR EFFICIENCIES FOR THE $^{58}Ni(n,p)^{58}Co$, $^{115}In(n,n')^{115m}In$ AND $^{64}Zn(n,p)^{64}Cu$ REACTIONS FOR 2.5 MEV NEUTRONS AND THE $^{63}Cu(n,2n)^{62}Cu$ AND $^{28}Si(n,p)^{28}Al$ REACTIONS FOR 14 MEV NEUTRONS.

Reaction	Atomic Mass	Isotopic Abundance	Half-Life	E_γ (keV)	Branching Ratio	Detector Efficiency
$^{115}In(n,n')^{115m}In$	114.82	0.957	4.486h	336	0.459 ±0.002	0.0358 ±0.0011
$^{58}Ni(n,p)^{58}Co$	58.69	0.6827	70.82d	811	0.994 ±0.002	0.0123 ±0.0004
$^{64}Zn(n,p)^{64}Cu$	65.39	0.486	12.70h	511	0.3580	0.0177 ±0.0005
$^{28}Si(n,p)^{28}Al$	28.085	0.9223	2.244m	1779	1.000	0.0128 * ±0.0013
$^{63}Cu(n,2n)^{62}Cu$	63.55	0.6917	9.74m	511	1.9486	0.0173 ±0.0005

*NaI scintillator efficiency.

Table VII

CORRECTIONS TO THE ACTIVATION COEFFICIENTS COMPUTED WITH MCNP FOR A 20 KeV MAXWELLIAN PLASMA, AS APPROPRIATE TO THE CONDITIONS FOR JET DISCHARGES

Reaction	Adjustment to σ_{Watt} = 312 mb for $^{238}U(n,f)$	$\frac{\sigma_{JET}}{\sigma_{MCNP}}$ *	14 MeV * correct. factor	Adjustment for height wrt 194.5 cm.	Corrected MCNP $\langle\sigma\phi\rangle$ for new irr. ends (± 5%)
$^{58}Ni(n,p)$	N/A	1.04	1.010	0.998	8.40E-32
$^{64}Zn(n,p)$	N/A	1.10	1.050	0.998	2.49E-32
$^{63}Cu(n,2n)$	N/A	N/A	N/A	0.998	2.31E-31×
$^{115}In(n,n')$	1.035 ± 0.021	1.00	0.991	0.998	2.99E-31
$^{232}Th(n,f)$	1.044 ± 0.024	1.00	1.014	0.975	1.09E-31
$^{238}U(n,f)$	1.000 ± 0.021+	1.00	1.006	0.983	4.67E-31

*Typical values quoted; actual values vary for each discharge.
There are additional corrections of up to 2% for varying plasma position.
+The uncertainty for ^{238}U should additionally be applied to ^{115}In and ^{232}Th.
×Computed for 14 MeV neutrons.

Table VIII

RESULTS OF THE 2.5 MEV ACTIVATION MEASUREMENTS, INCLUDING CORRECTIONS FOR 14 MEV NEUTRON CONTRIBUTION AND VESSEL EXPANSION.

Material	Discharge	Heating Power (MW)		Neutron Yield Ratios	
		NBI	ICRF	Delayed neutrons / Fission chambers	Activation / Fission chambers
Indium	20910	17	7	1.16	1.23
	20930	6	9	1.12	1.16
	20933	15	-	1.12	1.01
	20934	17	7	1.14	1.20
	20977	16	-	1.12	1.11
Nickel	20798 - 20802	16	2	1.12	1.01
	20925 - 20927	15	8	1.11	1.16
	20953 - 20958	16	4	1.10	1.19
Zinc	20915	10	-	1.07	1.34
	20928	16	8	1.16	1.45
	20929	16	7	1.13	1.37

Averaged 2.5 MeV neutron yield ratios from Octant 3 results:

1. Delayed neutrons (thorium) / fission chambers = 1.12 ± 0.02
2. Indium activation / fission chambers = 1.14 ± 0.04
3. Nickel activation / fission chambers = 1.12 ± 0.05
4. Zinc activation / fission chambers = 1.39 ± 0.03

The statistical errors associated with the above individual measurements are typically less than 1% .

Table IX

RELATIVE RESPONSES MEASURED IN THE EIGHT IRRADIATION ENDS, FOR 2.5 MEV AND 14 MEV NEUTRONS.

Method	Position of Irradiation End							
	Outboard				Central	Inboard		
	2-U	2-L	6-U	6-L	3-L	4-U	8-U	8-L
2.5 MeV Neutrons								
Delayed neutrons:								
Thorium	0.484	0.480	0.484	0.475	1.000	0.314	0.323	-
Uranium	0.486	0.492	0.469	-	-	0.319	-	
	0.485	0.486	0.481	0.475	1.000	0.317	0.323	
14 MeV Neutrons								
Silicon	-	0.465	0.486	0.474	1.000	-	-	0.321
Copper				0.465	1.000			0.295

N.B. The accuracy of the count-rate ratios quoted above is everywhere better than 2%. The relative responses have been corrected to a standard sample height in Octant 3-L of 194.5 cm.in a hot vessel.

Effective activation coefficients for comparison with Table III:

	Inboard	Central	Outboard
Indium at 2.5 MeV:	0.93-31	2.92-31	1.41-31
Zinc at 2.5 MeV:	(0.60-32)	(1.89-32)	(0.91-32)
Copper at 14 MeV:	0.68-31	2.31-31	1.07-31

Table X

ACCURACY OF THE NEUTRON YIELD MEASUREMENTS

1. Fission Chambers: Absolute calibration to be determined

2.

	Delayed Neutrons		Gamma Measurements (Indium)	Gamma Measurements (Copper)
Detector Efficiency	± 0.9%		± 3.0%	± 3.0%
Integral Cross-Section	-		± 2.1%	
Point Cross-Section	-		-	± 4.0%
Measurement Reproducibility	± 1.5%		± 4.0%	± 2.5%
	± 1.8%		± 5.4%	± 5.6%
^{238}U Point Cross-Sections		± 3.0%		-
Activation Coeff. (systematic)		± 5.0%		± 5.0%
Activation Coeff. (random)		-		± 3.0%
		± 5.8%		
Absolute error	± 6.1%		± 7.9%	± 8.1%

3. Uncertainties in Point Cross-Section Data:

^{58}Ni(n,p)	at 2.5 MeV	± 10%
^{64}Zn(n,p)	at 2.5 MeV	± 12%
^{115}In(n,n')	at 2.5 MeV	± 15%
^{232}Th(n,f)	at 2.5 MeV	± 5%
^{238}U(n,f)	at 2.5 MeV	± 3%
^{63}Cu(n,2n)	at 14 MeV	± 6%

The code NJOY has been used to process the covariance data in the ENDF/B-V and ENDL data libraries (on which DOSCROS84 is based). The resulting uncertainties, shown above, represent the spreads in the measured values of the original experimental results. The standard errors should be smaller.

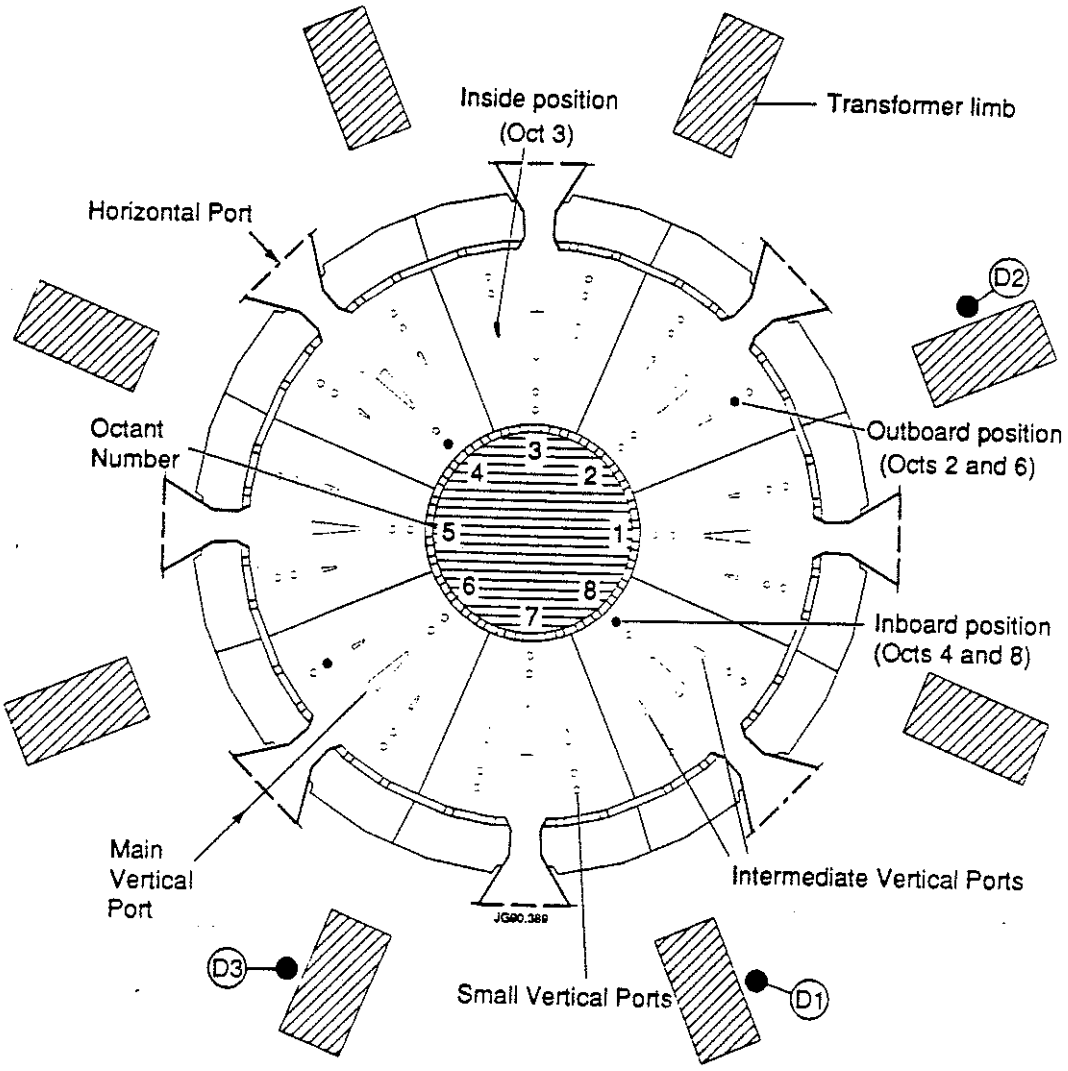

Fig 1. Section of JET at the horizontal mid plane, showing the positions of the fission chambers and of the irradiation ends.

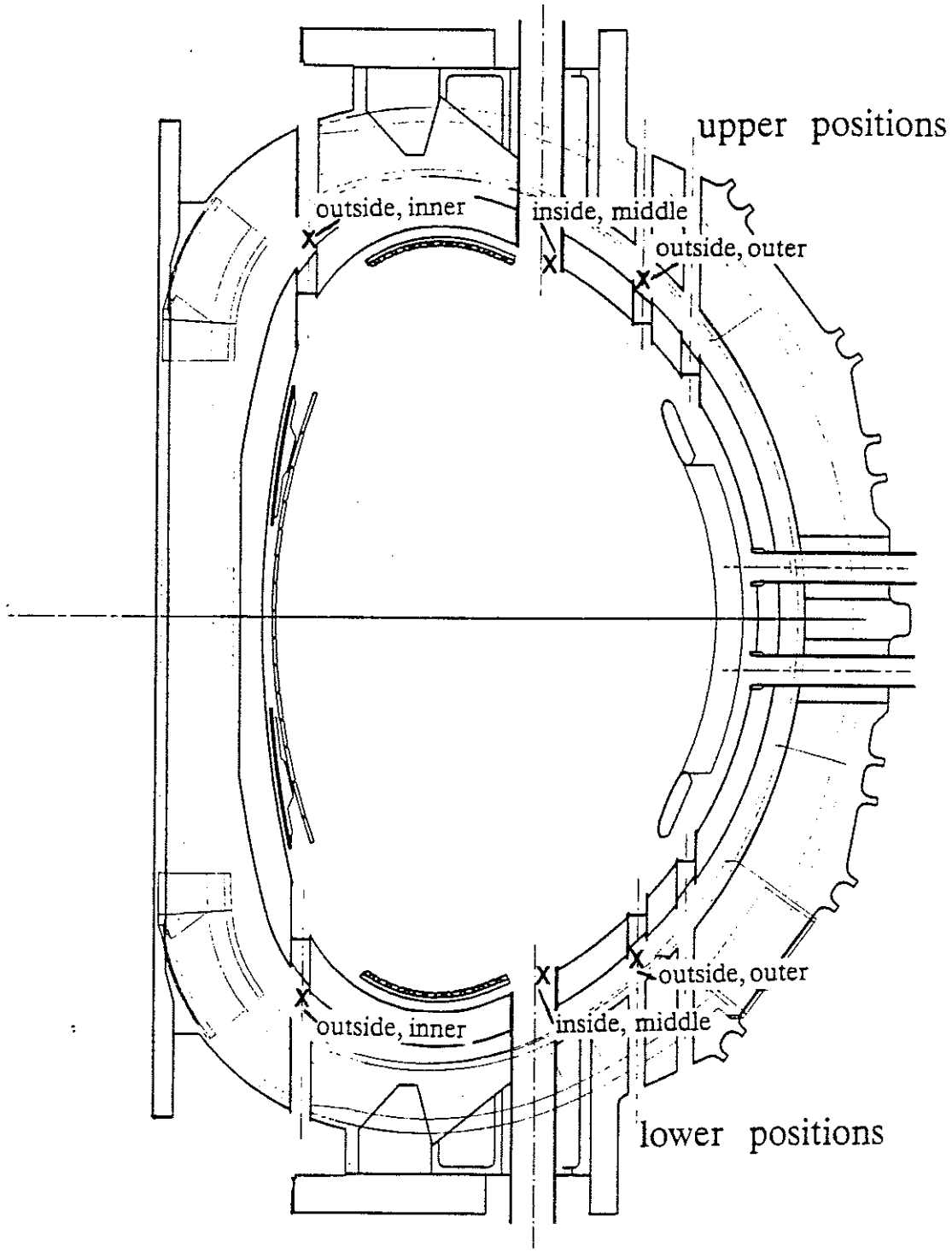

Fig 2. A drawing of a vertical section through the JET vacuum vessel, showing the location of the irradiation ends.

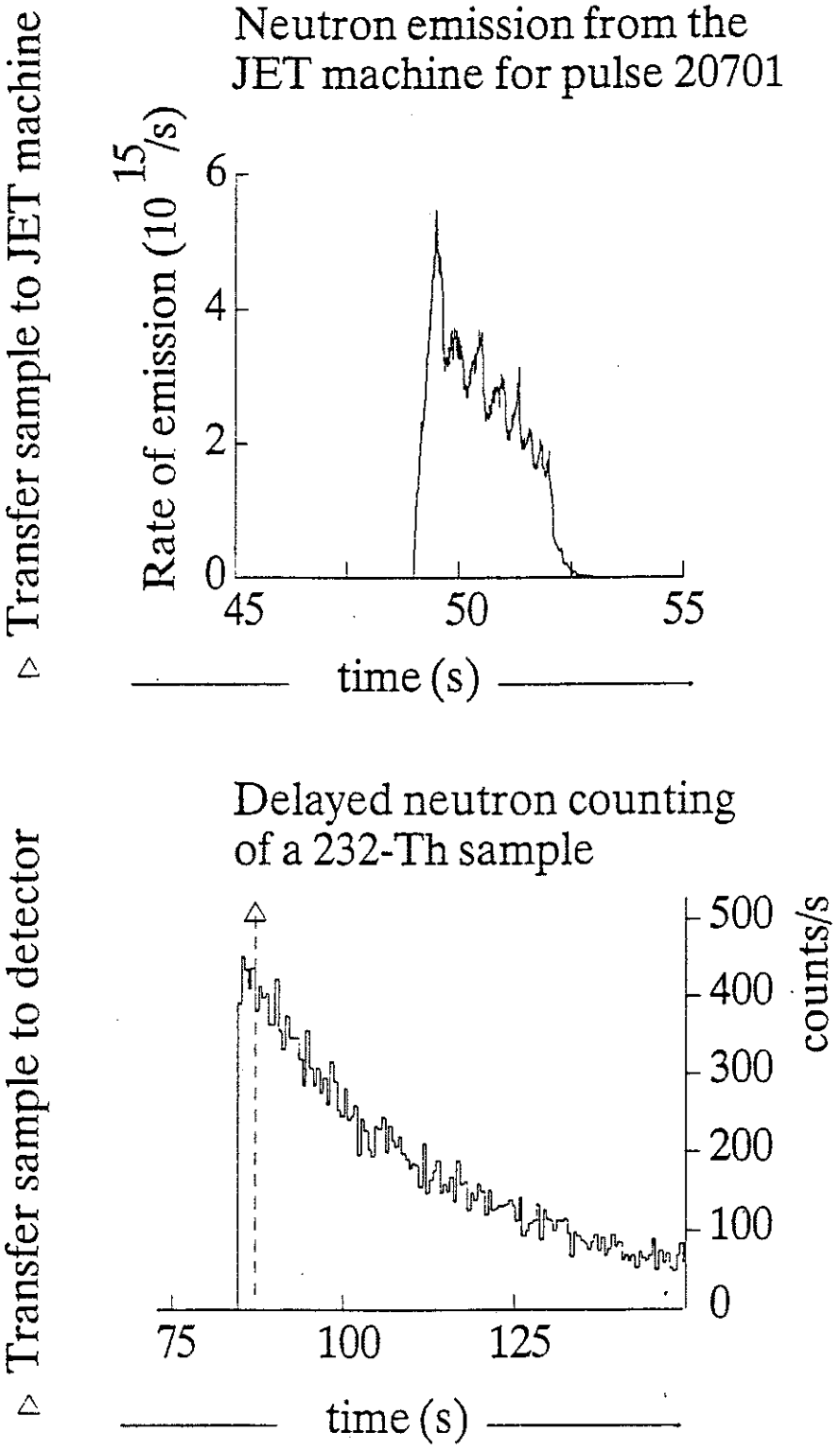

Fig 3. Illustrating the time sequence involved in the use of the delayed neutron counting system for a typical JET discharge.

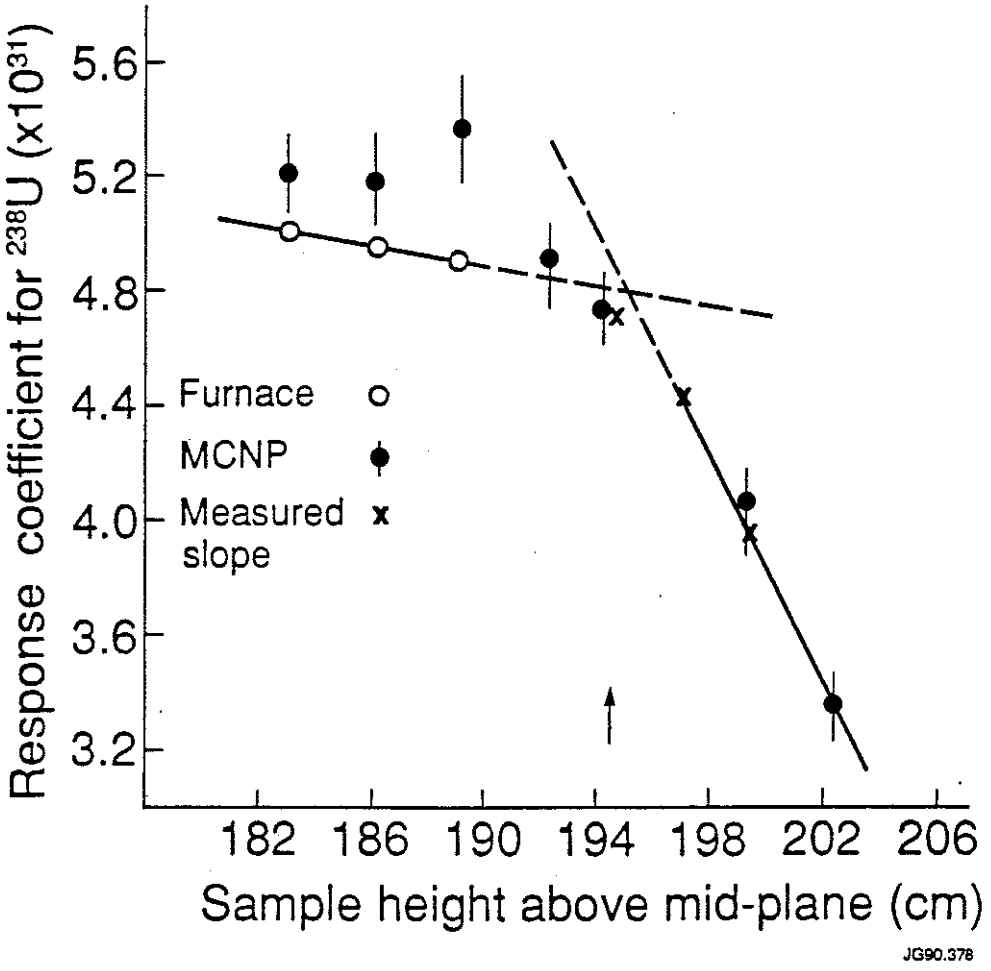

Fig 4. Showing the variation of the ^{238}U response coefficient as a function of height above the tokamak horizontal midplane. The results of FURNACE and MCNP transport codes are compared and measurements of the gradient above the operating position are fitted to the MCNP data.
The coefficient at 194.5 cm. is taken to be $4.74 \times 10^{-31} \pm 5\%$.

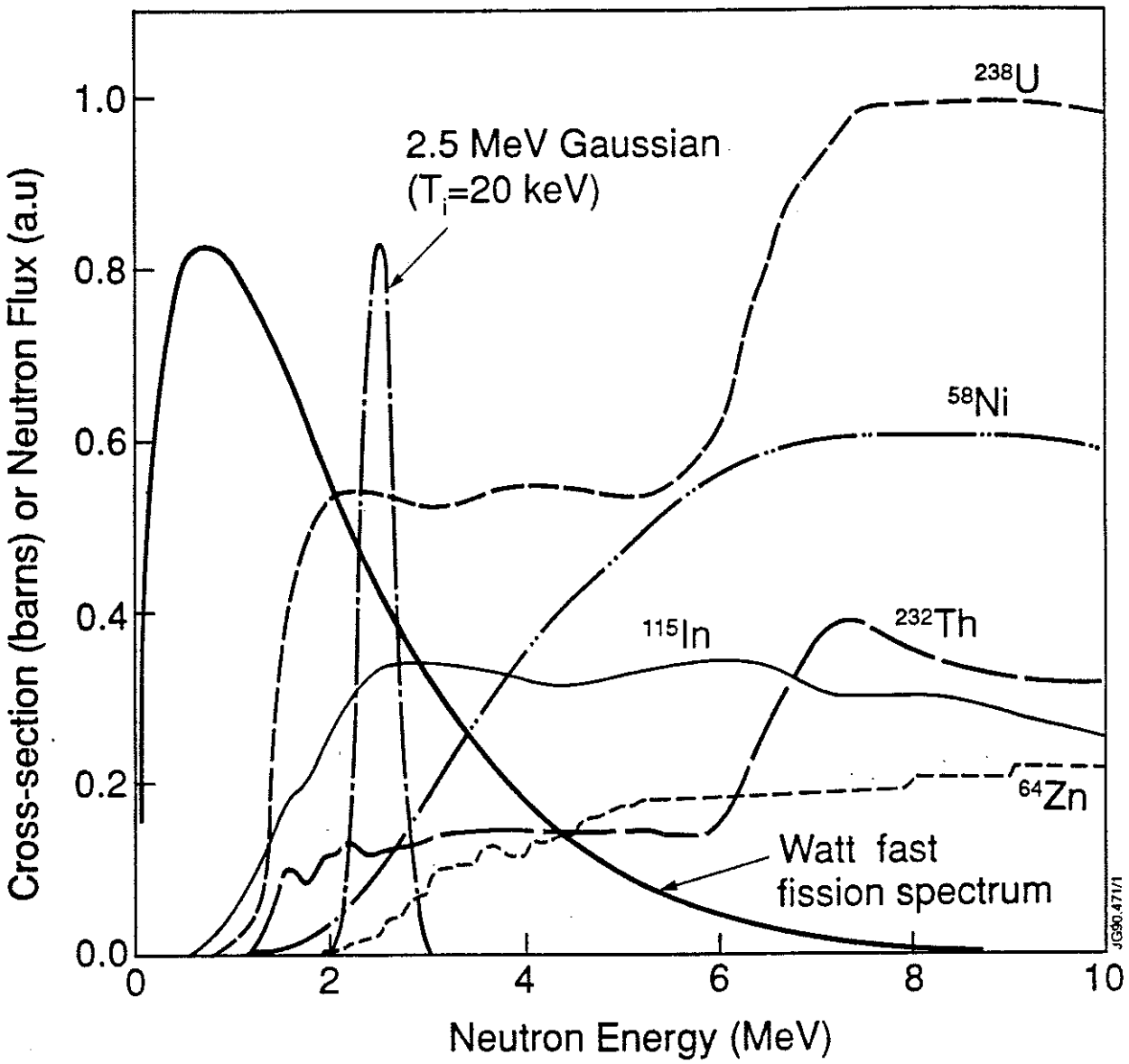

Fig 5. Showing the cross-sections for the reactions used in the measurement of 2.5 MeV neutron fluxes; also shown are the Watt fast fission neutron energy spectrum and the Gaussian representing the 2.5 MeV neutrons from d-d fusion reactions.

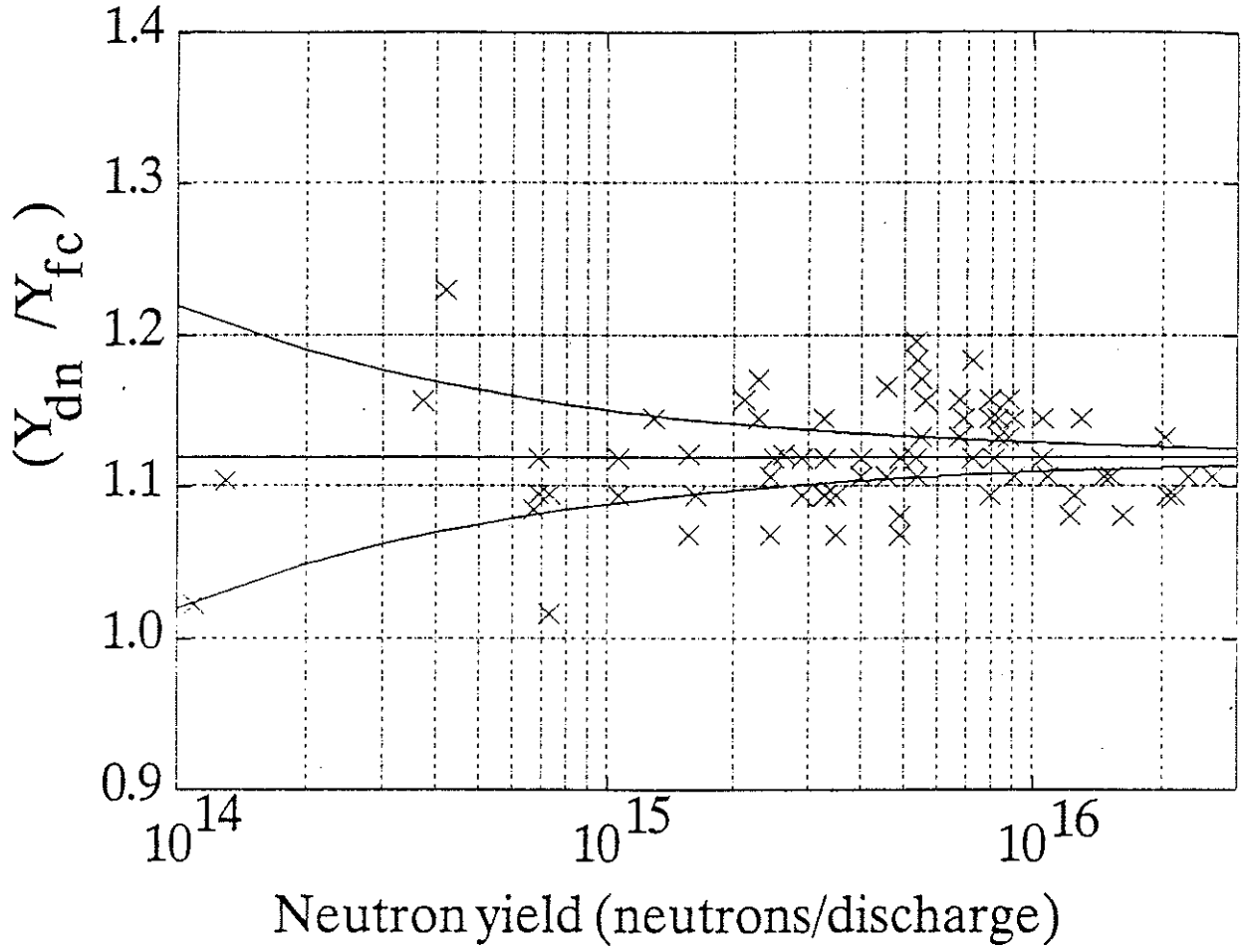

Fig 6. The ratio of delayed neutron/fission chamber neutron yields as a function of neutron emission strength. The solid curves indicate the ± 2 s.d. uncertainties attributable to counting statistics.

APPENDIX 1.

THE JET TEAM

JET Joint Undertaking, Abingdon, Oxon, OX14 3EA, U.K.

J.M.Adams[1], F.Alladio[4], H.Altmann, R.J.Anderson, G.Appruzzese, W.Bailey, B.Balet, D.V.Bartlett, L.R.Baylor[24], K.Behringer, A.C.Bell, P.Bertoldi, E.Bertolini, V.Bhatnagar, R.J.Bickerton, A.Boileau[3], T.Bonicelli, S.J.Booth, G.Bosia, M.Botman, D.Boyd[31], H.Brelen, H.Brinkschulte, M.Brusati, T.Budd, M.Bures, T.Businaro[4], H.Buttgereit, D.Cacaut, C.Caldwell-Nichols, D.J.Campbell, P.Card, J.Carwardine, G.Celentano, P.Chabert[27], C.D.Challis, A.Cheetham, J.Christiansen, C.Christodoulopoulos, P.Chuilon, R.Claesen, S.Clement[30], J.P.Coad, P.Colestock[6], S.Conroy[13], M.Cooke, S.Cooper, J.G.Cordey, W.Core, S.Corti, A.E.Costley, G.Cottrell, M.Cox[7], P.Cripwell[13], F.Crisanti[4], D.Cross, H.de Blank[16], J.de Haas[16], L.de Kock, E.Deksnis, G.B.Denne, G.Deschamps, G.Devillars, K.J.Dietz, J.Dobbing, S.E.Dorling, P.G.Doyle, D.F.Düchs, H.Duquenoy, A.Edwards, J.Ehrenberg[14], T.Elevant[12], W.Engelhardt, S.K.Erents[7], L.G.Eriksonn[5], M.Evrard[2], H.Falter, D.Flory, M.Forrest[7], C.Froger, K.Fullard, M.Gadeberg[11], A.Galetsas, R.Galvao[8], A.Gibson, R.D.Gill, A.Gondhalekar, C.Gordon, G.Gorini, C.Gormezano, N.A.Gottardi, C.Gowers, B.J.Green, F.S.Griph, M.Gryzinski[26], R.Haange, G.Hammett[6], W.Han[9], C.J.Hancock, P.J.Harbour, N.C.Hawkes[7], P.Haynes[7], T.Hellsten, J.L.Hemmerich, R.Hemsworth, R.F.Herzog, K.Hirsch[14], J.Hoekzema, W.A.Houlberg[24], J.How, M.Huart, A.Hubbard, T.P.Hughes[32], M.Hugon, M.Huguet, J.Jacquinot, O.N.Jarvis, T.C.Jernigan[24], E.Joffrin, E.M.Jones, L.P.D.F.Jones, T.T.C.Jones, J.Källne, A.Kaye, B.E.Keen, M.Keilhacker, G.J.Kelly, A.Khare[15], S.Knowlton, A.Konstantellos, M.Kovanen[21], P.Kupschus, P.Lallia, J.R.Last, L.Lauro-Taroni, M.Laux[33], K.Lawson[7], E.Lazzaro, M.Lennholm, X.Litaudon, P.Lomas, M.Lorentz-Gottardi[2], C.Lowry, G.Magyar, D.Maisonnier, M.Malacarne, V.Marchese, P.Massmann, L.McCarthy[28], G.McCracken[7], P.Mendonca, P.Meriguet, P.Micozzi[4], S.F.Mills, P.Millward, S.L.Milora[24], A.Moissonnier, P.L.Mondino, D.Moreau[17], P.Morgan, H.Morsi[14], G.Murphy, M.F.Nave, M.Newman, L.Nickesson, P.Nielsen, P.Noll, W.Obert, D.O'Brien, J.O'Rourke, M.G.Pacco-Düchs, M.Pain, S.Papastergiou, D.Pasini[20], M.Paume[27], N.Peacock[7], D.Pearson[13], F.Pegoraro, M.Pick, S.Pitcher[7], J.Plancoulaine, J-P.Poffé, F.Porcelli, R.Prentice, T.Raimondi, J.Ramette[17], J.M.Rax[27], C.Raymond, P-H.Rebut, J.Removille, F.Rimini, D.Robinson[7], A.Rolfe, R.T.Ross, L.Rossi, G.Rupprecht[14], R.Rushton, P.Rutter, H.C.Sack, G.Sadler, N.Salmon[13], H.Salzmann[14], A.Santagiustina, D.Schissel[25], P.H.Schild, M.Schmid, G.Schmidt[6], R.L.Shaw, A.Sibley, R.Simonini, J.Sips[16], P.Smeulders, J.Snipes, S.Sommers, L.Sonnerup, K.Sonnenberg, M.Stamp, P.Stangeby[19], D.Start, C.A.Steed, D.Stork, P.E.Stott, T.E.Stringer, D.Stubberfield, T.Sugie[18], D.Summers, H.Summers[20], J.Taboda-Duarte[22], J.Tagle[30], H.Tamnen, A.Tanga, A.Taroni, C.Tebaldi[23], A.Tesini, P.R.Thomas, E.Thompson, K.Thomsen[11], P.Trevalion, M.Tschudin, B.Tubbing, K.Uchino[29], E.Usselmann, H.van der Beken, M.von Hellermann, T.Wade, C.Walker, B.A.Wallander, M.Walravens, K.Walter, D.Ward, M.L.Watkins, J.Wesson, D.H.Wheeler, J.Wilks, U.Willen[12], D.Wilson, T.Winkel, C.Woodward, M.Wykes, I.D.Young, L.Zannelli, M.Zarnstorff[6], D.Zasche[14], J.W.Zwart.

PERMANENT ADDRESS

1. UKAEA, Harwell, Oxon. UK.
2. EUR-EB Association, LPP-ERM/KMS, B-1040 Brussels, Belgium.
3. Institute National des Récherches Scientifique, Quebec, Canada.
4. ENEA-CENTRO Di Frascati, I-00044 Frascati, Roma, Italy.
5. Chalmers University of Technology, Göteborg, Sweden.
6. Princeton Plasma Physics Laboratory, New Jersey, USA.
7. UKAEA Culham Laboratory, Abingdon, Oxon. UK.
8. Plasma Physics Laboratory, Space Research Institute, Sao José dos Campos, Brazil.
9. Institute of Mathematics, University of Oxford, UK.
10. CRPP/EPFL, 21 Avenue des Bains, CH-1007 Lausanne, Switzerland.
11. Risø National Laboratory, DK-4000 Roskilde, Denmark.
12. Swedish Energy Research Commission, S-10072 Stockholm, Sweden.
13. Imperial College of Science and Technology, University of London, UK.
14. Max Planck Institut für Plasmaphysik, D-8046 Garching bei München, FRG.
15. Institute for Plasma Research, Gandhinagar Bhat Gujat, India.
16. FOM Instituut voor Plasmafysica, 3430 Be Nieuwegein, The Netherlands.
17. Commissiariat à L'Energie Atomique, F-92260 Fontenay-aux-Roses, France.
18. JAERI, Tokai Research Establishment, Tokai-Mura, Naka-Gun, Japan.
19. Institute for Aerospace Studies, University of Toronto, Downsview, Ontario, Canada.
20. University of Strathclyde, Glasgow, G4 ONG, U.K.
21. Nuclear Engineering Laboratory, Lapeenranta University, Finland.
22. JNICT, Lisboa, Portugal.
23. Department of Mathematics, Univeristy of Bologna, Italy.
24. Oak Ridge National Laboratory, Oak Ridge, Tenn., USA.
25. G.A. Technologies, San Diego, California, USA.
26. Institute for Nuclear Studies, Swierk, Poland.
27. Commissiariat à l'Energie Atomique, Cadarache, France.
28. School of Physical Sciences, Flinders University of South Australia, South Australia SO42.
29. Kyushi University, Kasagu Fukuoka, Japan.
30. Centro de Investigaciones Energeticas Medioambientales y Techalogicas, Spain.
31. University of Maryland, College Park, Maryland, USA.
32. University of Essex, Colchester, UK.
33. Akademie de Wissenschaften, Berlin, DDR.

CR 88.49.1A